Materials Research Bulletin 146 (2022) 111612

Contents lists available at ScienceDirect

Materials Research Bulletin

journal homepage: www.elsevier.com/locate/matresbu

Review

Recent progress of perovskite-based electrolyte materials for solid oxide fuel cells and performance optimizing strategies for energy storage applications

Muhammad Bilal Hanif [a,b], Sajid Rauf [c], Martin Motola [b], Zaheer Ud Din Babar [a], Chang-Jiu Li [a], Cheng-Xin Li [a,*]

[a] State Key Laboratory for Mechanical Behavior of Materials, School of Materials Science and Engineering, Xi'an Jiaotong University, Xi'an, Shaanxi, China
[b] Department of Inorganic Chemistry, Faculty of Natural Sciences, Comenius University in Bratislava, Bratislava 84215, Slovakia
[c] College of Electronics and information Engineering, Shenzhen University, Guangdong 518000, China

ARTICLE INFO

Keywords:
Solid oxide fuel cells
Electrolyte materials
Energy storage applications
Doping strategies

ABSTRACT

Solid oxide fuel cells (SOFCs) are found to have potential application in energy conversion technology due to their characteristics i.e., good modularization, better fuel efficiency, and lesser toxic products (CO_2, SO_x, and NO_x). Mostly the electrolytic materials with ionic or protonic conductivity, undergo degradation at various operating conditions which must be prevented. Based on the above-mentioned problems, perovskites are considered as one of the wonderful classes of electrode and electrolyte materials with hydrocarbon fuels and retentivity of inherent stability at reducing/oxidizing atmosphere. In this review, recent developments in perovskite electrolyte materials of solid oxide fuel cells are summarized with prospects. Here, our main purpose is to deliver a brief tutorial corresponding to the structure, properties, and electrochemical behavior of perovskite-based electrolytes in test cells with various dopants together and inherited challenges regarding this material family. Several novel design strategies for the optimization of cell performance i.e., interface engineering, strain modulation, and defect engineering have been discussed in detail. In addition to this, a perspective has been proposed on the development routes or designs for perovskite oxide-based materials with high performance in energy conversion and storage applications as well as the way forward to cope with the challenges involved in the research route regarding the performance of each component.

1. Introduction

Rapid industrialization has increased the world's energy demand massively, being mainly fulfilled by fossil fuel burning. The two main concerns that arise in this situation include the depletion of fossil fuel reserves and the environmental impact triggered by associated greenhouse gasses. Hence, the researchers are focusing on finding an efficient alternative having higher energy content with lower environmental effects. In contrary to the conventional combustion scheme, the fuel and air combustion in fuel cells are less owing to its inherent higher electrical efficiencies. The fuel cell can skillfully and rapidly store electrical energy as hydrogen which is produced through high-temperature electrolysis when it works in the accelerative mode [1].

In 1839, Gustav Rose found a mineral named calcium titanium oxide ($CaTiO_3$) in the Ural Mountains of Russia. The term perovskite was given to this mineral in a tribute to a Russian scientist, Lev Perovski. All materials with the chemical form same as that of the perovskite $CaTiO_3$ were called a perovskite material. Perovskites denote a wonderful class of materials with fascinating properties which makes them an attractive option of research for researchers around the world. The common chemical form of a perovskite structure is ABX_3. A in the formula is for large cations while B represents smaller cations having coordination no of 12 and 6 respectively. Large cations may comprise of alkali, alkaline earth metals, rare earth, or other metals whereas, B represents various transition metals. Properties of perovskites depend upon the atoms/molecules used in their structure [2]. Cations with a wide range of ionic radii and valences can enter one or more sites in the perovskite structure, exhibiting a variety of chemical and physical characteristics, allowing for high oxide vacancy concentrations and strong ionic conductivity [3]. They are attractive candidates for electrodes in SOFC

* Corresponding author.
E-mail address: licx@mail.xjtu.edu.cn (C.-X. Li).

https://doi.org/10.1016/j.materresbull.2021.111612
Received 18 August 2021; Received in revised form 13 October 2021; Accepted 19 October 2021
Available online 26 October 2021

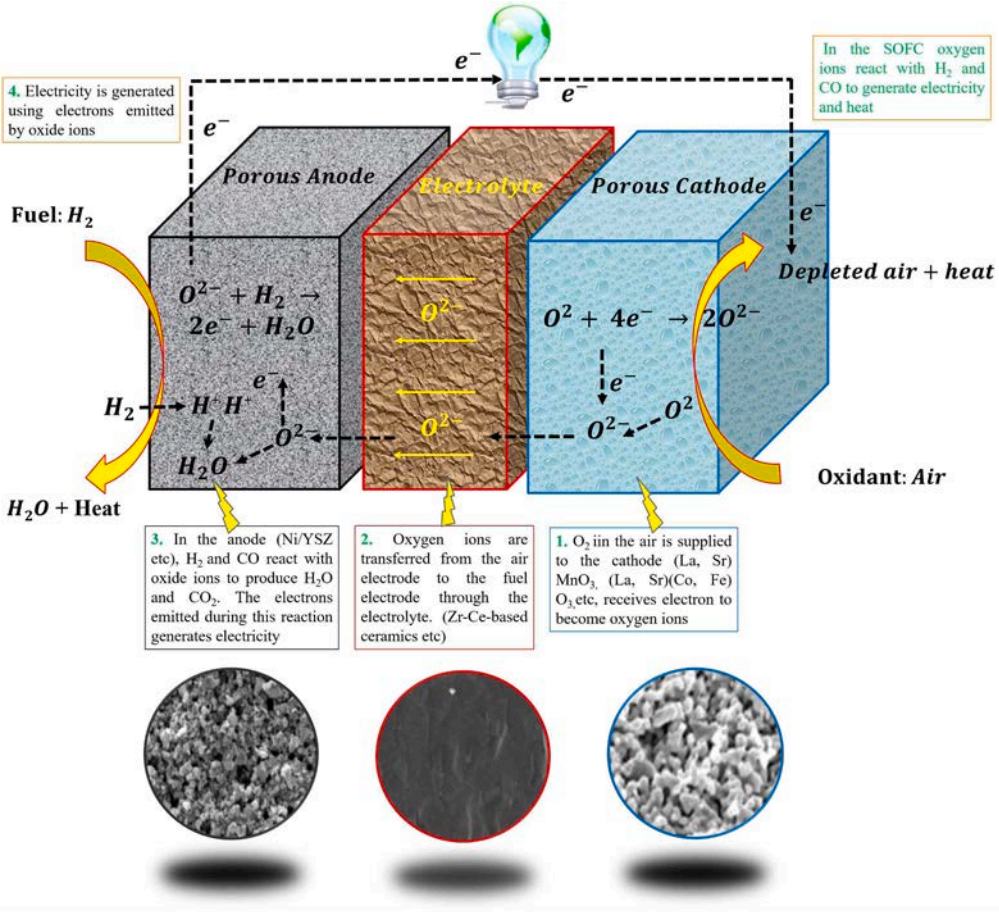

Fig. 1. Working principle of SOFC.

applications because of their capacity to hold a large number of oxygen vacancies. The B-cations are on the cube's corners, while the A-cation is in the center. The oxygen is inserted in the center of each of the twelve cube edges, resulting in BO_6 octahedra with shared corners. The size of the A-cation is the same as that of the oxide ion, whereas the B-cation is smaller. It is possible to create oxygen vacancies in the structure depending on the type of cations used. Ionic conduction is caused by these oxygen vacancies moving along the lattice. The composition and microstructure of electrode materials have a significant impact on SOFC performance. The high temperature, as well as the presence of oxidizing or reducing atmospheres, limit the materials that can be used.

In oxidation and reduction reactions, perovskites can act as catalysts. Their catalytic activity is mostly determined by the band structure and density of states. Perovskites with a transition metal B-site, such as cobalt, nickel, or copper, exhibit particularly strong catalytic activity [4]. The catalytic activity of an A-ion is normally inert, but its substitution with cations of different valences has an effect. Furthermore, the shape of the material and the availability of B-ions on the surface are essential in terms of catalytic process kinetics. Perovskite oxides are essential functional materials with good physical and chemical properties that are widely used in piezoelectric, ferroelectric, energy conversion, dielectric, and storage applications, among others [5].

SOFCs have the potential to be used in energy conversion technology. For its successful commercialization, steps should be taken for cost reduction and stability. The composition and microstructure of perovskite materials determine the electrochemical response of solid oxide fuel cells therefore, it requires a complete understanding of the reaction mechanism that occurs at the surface of the perovskite electrode in relation to the electrolyte. For electrochemical characterization of fuel cells, several studies have been performed comprising of classification, separation, and extent of loss of composition or mass [3–5].

SOFCs contain two electrodes (i.e., anode/cathode) that are porous and apart by a dense electrolyte. Cathode involves in a reaction with electrons from the exterior circuit, at cathode oxide ions are generated through the availability of oxygen which then further move towards the anode through the electrolyte. Anode facilitates the combination reaction between oxide ions with carbon monoxide (CO) or hydrogen (H_2) as a result carbon dioxide (CO_2) or water (H_2O) are formed with the release of electrons. Electrons that are released are responsible for the production of electricity through transfer from anode to cathode [6,7]. The reaction can be stated in Kröger Vink representation as follows. Eqs. (1)–((4)).

O_2 reduction reaction at the cathode:

$$\frac{1}{2}O_2 + 2e^- + V_{\ddot{O}} = O_O^x \quad (1)$$

At the anode, the fuel is oxidized.

$$H_2 + O_O^x = H_2O + 2e^- + V_{\ddot{O}} \quad (2)$$

$$CO + O_O^x = CO_2 + 2e^- + V_{\ddot{O}} \quad (3)$$

$$C_nH_{2n+2} + (3n+1)\,O_O^x = nCO_2 + (n+1)H_2O + (6n+2)e^- + (3n+1)V_{\ddot{O}} \quad (4)$$

Whereas,

$V_{\ddot{O}}$ = Oxygen vacancies, O_O^x= O_2-ions on a regular O_2-site in the electrolyte lattice. Fig. 1. illustrates the working principle of SOFCs.

The standard electrochemical reactions that occurred at the anode and cathode are mentioned below:

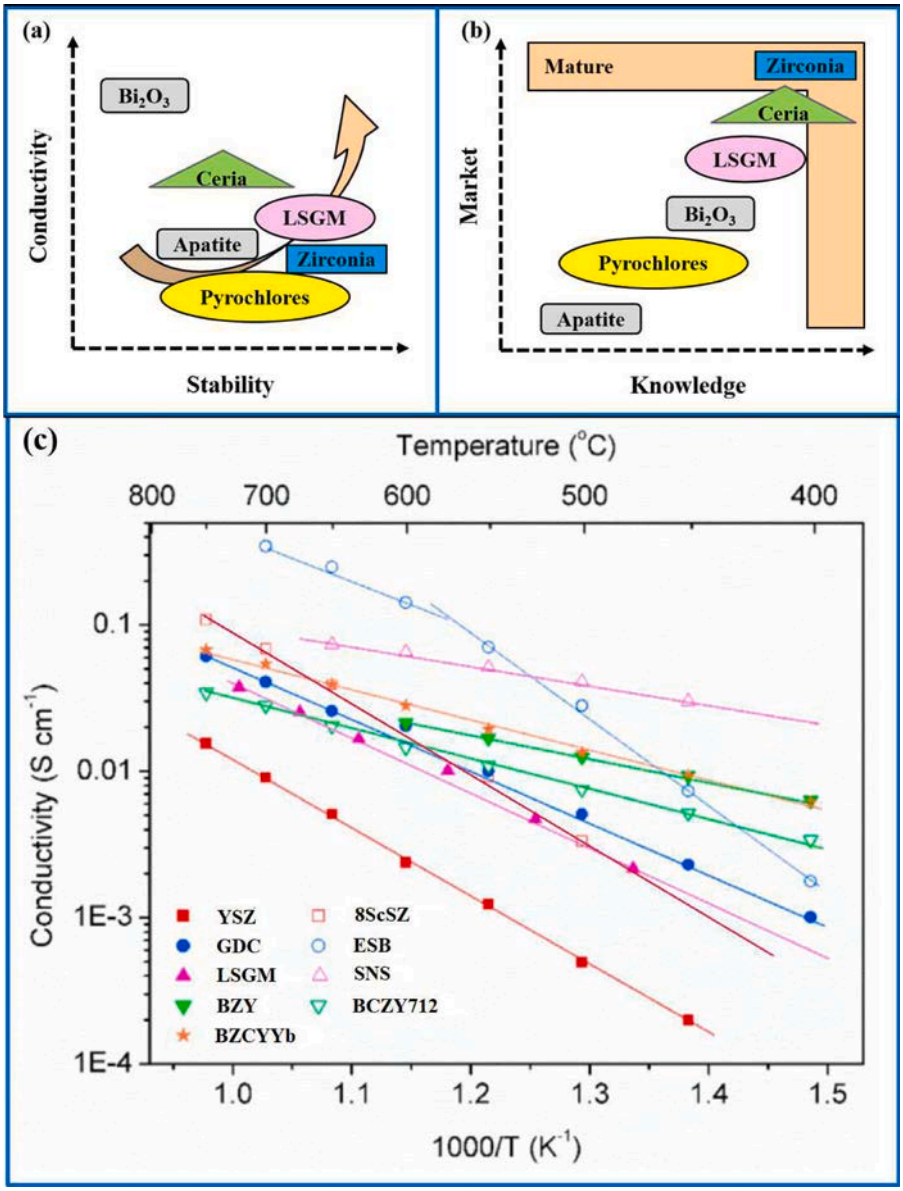

Fig. 2. Conductivity Vs stability graph (a, b) along with an enormous amount of information available on several families of materials. (c) comparison of ionic conductivity of various electrolytes which includes 8ScSZ [27], YSZ [28], LSGM [29], GDC [16], BZCYYb [30], BCZY [31], BZY [32], SNS [12] and ESB [33] respectively.

$$\text{Anode}: O^{2-} + H_2 \rightarrow 2e^- + H_2O \quad (5)$$

$$\text{Cathode}: O^2 + 4e^- \rightarrow 2O^{2-} \quad (6)$$

$$\text{Overall}: \frac{1}{2}O_2 + H_2 \rightarrow H_2O \quad (7)$$

Numerous liquid oxygenated hydrocarbons comprising of acetic acid, ethylene glycol, ethanol, methanol, and glycerol are suitable for use as fuels in SOFCs either by direct utilization or through internal reforming/partial oxidation [8–12]. In the fabrication of SOFCs, Ni-based cermet's are found to be the most widely used anode material, imparting stability and efficient activity of electrochemical oxidation reaction [13]. However, there are some issues with its application, such as Ni deposition due to low resistivity, which leads to cell deterioration [14,15]. This shows that, in the quest for alternative fuels, careful design of coking-resistant anodes is required to commercialize hydrocarbon-fueled SOFCs. Several papers are now being written to develop anode fabrication methodologies, anode kinetic investigations, and anodic reaction processes for SOFCs [16–20].

Whereas, cathode materials based on lanthanum strontium manganite (LSM) have been reported for significant performance at elevated temperatures (1000 °C). Whereas, low temperatures (600 °C) support the higher activation energy of ORR, making SOFCs (IT-SOFCs) unsuitable for intermediate temperature range functioning because polarization resistance (Rp) was influenced and increased with lower operating temperatures for SOFCs [21,22]. Several mixed conducting materials including, $La_{0.6}Sr_{0.4}Co_{0.2}Fe_{0.8}O_{3-\delta}$ (LSCF), $Ba_{0.5}Sr_{0.5}Co_{0.8}Fe_{0.2}O_{3-\delta}$ (BSCF), solid solutions of doped $LaMnO_3$ with $La_{1-x}Sr_xCuO_3$, $LaCrO_3$, $LaCoO_3$, and have been reported as cathode materials. These materials are responsible for the remarkable increase in the active area for reducing oxygen [23,24]. However, to commercialize SOFCs, researchers are concentrating on the creation of low-cost materials. So, to overcome the cost barrier, symmetric solid oxide fuel cells have emerged as a viable option, as these cells are constructed utilizing comparable materials for the cathode and anode [25]. There are numerous advantages to using this innovative strategy. Sulfur poisoning

and the development of coke at the anode can be eliminated without causing damage to the cell, which improves the stability and life cycle of fuel cells. Because the cathode and anode materials are identical, the manufacturing process involves only one step of heating. Many systematic reviews on recent improvements in cathodes and anodes for SOFCs are available in the literature, while the electrolyte has received less attention.

Recent advances in perovskite electrolyte materials for solid oxide fuel cells are discussed in this article, along with their prospects. The selection of initial composition, dopants, and electrolytes with critical challenges inherent to this material family has been assessed herein which plays a vital role in enhanced electrochemical performance. Novel performance optimization strategies, strain modulation, interface/defect engineering are also discussed. A detailed perspective was given on the development routes or designs for perovskite oxide-based materials for their enhanced performance in energy conversion and storage applications. Descriptive studies were performed to analyze the importance of perovskites materials in storage and energy conversion applications which could be a climacteric approach towards the advancement of SOFC.

2. Effect of dopants addition on ionic conductivity

The ionic conductivity of electrolytes depends upon many factors such as defect dissociation, temperature, dopant-concentration, sample preparation, and oxygen partial pressure. The Arrhenius relationship can be used to represent the temperature dependence of ionic conductivity.

$$\sigma T = A exp\left(-\frac{E_a}{kT}\right) \tag{8}$$

where, T, E_a, k, and A are the temperature, activation energy, Boltzmann constant, and the pre-exponential coefficient for the ionic conduction, respectively. Ionic conductivity can be expressed in terms of mobility (I), charge (q), charge carrier concentration (Ci), and for any given material. The relationship can be stated as follows:

$$\sigma_i = C_i q_i \mu_i \tag{9}$$

For pure oxide-ion conductors, Ci is the oxide ions concentration and can be presented by the number of oxide-ions present in the crystal per unit volume (N_o), and the site fraction of oxygen vacancies ($V_o^{\cdot\cdot}$).

$$C_i = \left(1 - \left[V_o^{\cdot\cdot}\right]\right) N_o \tag{10}$$

However, ionic mobility can be characterized by using the ion's diffusivity (Di) as follows:

$$\mu_i = \frac{q_i D_i}{kT} \tag{11}$$

However, the diffusivity term can be written and extended in terms of enthalpy entropy (ΔS_m) and (ΔH_m) of migration, lattice-vibration frequency (V_o), ion jump distance (a), and last but not least is oxygen vacancy concentration per unit volume ($[V_o^{\cdot\cdot}]N_o$)

$$D_i = a^2 v_o \left(\left[V_o^{\cdot\cdot}\right]\right) N_o exp\left(\frac{\Delta S_m}{k}\right) exp\left(-\frac{\Delta H_m}{kT}\right) \tag{12}$$

The accurate expression for the Arrhenius relationship can be achieved by adding Eqs. ((10)–(12)) into (9).

$$\sigma_i T = A\left[V_o^{\cdot\cdot}\right]\left(1 - \left[V_o^{\cdot\cdot}\right]\right) exp\left(-\frac{\Delta H_m}{kT}\right) \tag{13}$$

Whereas,

$$A = \left(\frac{4e^2}{k}\right) a^2 v_o N_o exp\left(\frac{\Delta S_m}{k}\right) \tag{14}$$

For very small values of $[V_o^{\cdot\cdot}]$, Eq. (15) becomes

$$\sigma_i T = A\left[V_o^{\cdot\cdot}\right] exp\left(-\frac{\Delta H_m}{kT}\right) \tag{15}$$

Kilner and Walters [26] define the actual temperature dependence of ionic conductivity as three distinct temperature regions. High temperatures are associated with region I. The intrinsic ionic defects (i.e., anion Frenkel) in the host crystal lattice dictate the ionic conductivity in this region. Intermediate temperatures are associated with region II. The charge carrying concentration of defects can be estimated by the content of acceptor impurity present in the material, which governs ionic conductivity in this regime. Region III is associated with low temperature, where the ionic conductivity is largely determined by the equilibrium between the associated pairs and concentration of charge-carrying defects. Thus, ionic conductivity in regions III and II is caused by the presence of mobile oxygen vacancies, which are primarily determined by the content acceptor impurity in the material. Based on the above-mentioned equations and Kilner and Walters [26] concepts, Fig. 2 (c) shows the comparison of ionic conductivity of various electrolytes (YSZ (8mol% Y_2O_3-ZrO_2), LSGM ($La_{0.8}Sr_{0.2}Ga_{0.8}Mg_{0.2}O_{3-\delta}$), 8ScSZ, ESB ($Er_{0.4}Bi_{0.6}O_3$), SNS ($Sr_{0.55}Na_{0.45}SiO_{2.755}$), BZY ($BaZr_{0.8}Y_{0.2}O_{3-\delta}$), BCZY ($BaZr_{0.1}Ce_{0.7}Yb_{0.1}O_{3-\delta}$), BCZYYb ($BaZr_{0.1}Ce_{0.7}Yb_{0.1}O_{3-\delta}$), respectively). Whereas, Fig. 2(a) depicts the impression that properties show a perpendicular tendency towards wanted admixture properties (a pink-peach arrow signifying higher conductivity and stability). Fig. 2(b) assists the immediate recognition which recommends that irrespective of a broad range of information accessible for several classes of materials these materials are still not being considered for technical applications.

According to the literature, ionic conductivity initially increases with increasing concentrations of acceptor dopant cations in ZrO_2-based systems. When the dopant concentration reaches its minimum level (i.e., low stabilization limit) required to completely stabilize the cubic fluorite structure of ZrO_2 then the conductivity shows its maximum. However, both the ionic conductivity and low-stabilization limit are influenced by the microstructural and thermo-mechanical characteristics which include grain boundaries cleanliness, dopants segregation, presence of metastable phases, and other impurities respectively. However, it is commonly recognized that the ionic conductivity of $(Y_2O_3)_x$-$(ZrO_2)_{1-x}$ is greatest when the Y_2O_3 content is around 8 mol.%. This 8 mol.% Y_2O_3 stabilized ZrO_2 is a well-known electrolyte for SOFCs operating at high temperatures (1000 °C). While a further increase in the dopant concentration hinders the flow of mobile oxygen vacancies that results in a decrease in ionic conductivity [34]. Whereas, the increase in the ionic conductivity is observed when Sc^{3+} is used as a dopant due to its ionic radii closer to Zr^{4+}. The temptation to form local defect associates tends to increase as the size of the dopant increases, resulting in a decrease in ionic conductivity [35–41].

In CeO_2 based electrolytes, trivalent dopants have significantly higher conductivity than divalent dopants due to a lower CTE mismatch between the host cation (Ce^{4+}) and trivalent dopants [42]. Butler et al., [43] calculated that the effect of the relaxation of dopant cations in CeO_2 towards oxygen vacancy tends to occur in the case of smaller-sized dopant cations, such as, Y^{3+} ($r^{3+}_{Yb,\ VIII} = 1.019$ Å), Sc^{3+} ($r^{3+}_{Sc,\ VIII} = 0.84$ Å), which increases its stability. Whereas, when the oxygen vacancy is introduced into the adjacent sites of larger-sized dopants such as La^{3+}($r^{3+}_{Gd,\ VIII} = 1.18$) and Gd^{3+}($r^{3+}_{Gd,\ VIII} = 1.053$) it will result in the decrease of elastic strain. The two conflicting outcomes occur in the lowest binding energy (0.17 eV) for Gd^{3+}. The calculated binding energies for Ce^{3+}, Sc^{3+}, La^{3+}, and Y^{3+} are 0.25, 0.62, 0.26, 0.38 eV respectively.

According to Kilner et al. [44] doped-fluorite structured shows maximum conductivity when the lattice elastic strain is negligible. Based on Kilner's supposition, dopants with an ionic radius closer to r_c should have a low association enthalpy and thus a high ionic conductivity. Using similar reasoning, Kim proposed that Gd^{3+} has the highest

Table 1
Doping and co-doping parameters which effects the ionic conductivity of respective SOFC electrolytes.

Composition	Operating Temp(°C)	TEC1 × 10^6 (/K).	Conductivity (Scm^{-1})	Remarks	Ref
Zirconia based electrolytes					
8-mol.% Y_2O_3- ZrO_2 (8YSZ)	1000	—-	0.13	Spray drying of nitrate solution was used in the process.	[28]
9.5-mol.% Y_2O_3-ZrO_2 (9.5YSZ)	900	—-	0.057	Magnetic pulse compaction of tapes cast of nano powders yielded a 15 to 25 μm-thick film.	[47]
10-mol.% Y_2O_3- ZrO_2(10YSZ)	400	10.6	4.52×10^{-6}	Atomic laser deposition was used to develop a 300 nm-thick film.	[48]
10.5-mol.% Y_2O_3-ZrO_2 (10.5YSZ)	800	—-	0.034	Aerosol assisted organic chemical-vapor deposition was used to prepare thin film	[49]
6 mol.% Sc_2O_3- ZrO_2 (6ScSZ)	1000	—-	0.18	To improve mechanical strength, hot isostatic-pressing was used to fabricate the dense coating.	[27]
9–11-mol.% Sc_2O_3-ZrO_2	1000	—-	0.28–0.34	Coprecipitated powders are sintered to develop this material.	[34]
CaO-ZrO_2+ 12.5 mol.% CaO	1000	—-	0.055	—-.	[50]
La_2O_3-ZrO_2+5 mol.% La_2O_3	1000	—-.	0.0044	—-.	[51]
Sc_2O_3–ZrO_2+6 mol.% Sc_2O_3	1000	—-.	0.18	To improve mechanical strength, hot isostatic-pressing (HIP) was used to fabricate the dense coating.	[52]
MgO-ZrO_2+13.7 mol.% MgO	1000	—-.	0.098	Traditional ceramic processing techniques such as pressing, wet mixing, machining, and sintering, are used to develop this material.	[52]
Ceria based electrolytes					
[a]$Ce_{0.85}Gd_{0.15}O_{2-\delta}$(15GDC) [b]$Ce_{0.9}Gd_{0.1}O_{2-\delta}$ (GDC) [c]$Ce_{0.8}Gd_{0.2}O_{2-\delta}$ (20GDC) [d]$Ce_{0.75}Gd_{0.25}O_{1.875}$ (25GDC)	[a] 700 [b] 27–827 [c] 50–1000 [d] 600	[b] 12.4 [b] 11.8 [c] 12.5	[a] 4.07×10^{-2} [d] 1.01×10^{-2}	[a] High purity Gd_2O_3 and CeO_2 powders were used as the starting materials. [b,c] Nanoparticles were uniaxially pressed into bulk pellets, followed by pressure less sintering [d] The flame spray pyrolysis method is used to create a solid solution.	[22–24]
[a1]$Ce_{0.8}Sm_{0.2}O_{1.9}$ (20SDC) [b]$Ce_{0.83}Sm_{0.17}O_{1.915}$ (17SDC)	[a1] 600 [a2] 800 [b] 600	8.6	[a1] 5×10^{-3} [a2]8.8×10^{-2} [b] 5.7×10^{-3}	[a1] The sol-gel method was used to create a solid solution of $Ce_{0.8}Sm_{0.2}O_{1.9}$. [a2] The powder was developed using the oxalate coprecipitation method. [b] Fabricated by hydrothermal route	[18]
$Ce_{0.8}Y_{0.2}O_{1.9}$ (20YDC)	700	—-	3.4×10^{-2}	It is made using the citric-acid nitrate, low-temperature combustion technique.	[53]
$Ce_{0.8}Sm_{0.1}Nd_{0.1}O_{1.9}$	500	—-	0.012	co-doped-ceria powder (Nd^{3+} and Sm^{3+}) were developed by the citric acid combustion method. The bulk sample was produced by sintering it at 1400 °C.	[20]
$Zr_{0.75}Ce_{0.08}Nd_{0.17}O_{1.9}$	~x223C 600	—-	3×10^{-4}	Solid-state sintering	[54]
Ca,Na-doped CeO_2	~x223C 600	—-	10^{-2}–10^{-1}	Sol-gel spin coating was used to develop a thin-film electrolyte of 0.1–0.6 μm.	[55]
$LaAlO_3$ and $LaGaO_3$-based electrolytes					
[a]$La_{0.8}Sr_{0.2}Ga_{0.8}Mg_{0.2}O_{3-\delta}$ [b]$La_{0.9}Sr_{0.1}Ga_{0.8}Mg_{0.2}O_{3-\delta}$	[a] 300–800 [b] 800	[a] 12.4 [b] 11.9 (27–1200 °C)	[a] 0.45–0.025 [b] 10.2	[a] The powders were compacted, then isostatically pressed and sintered in air.	[56–59]
$La_{0.8}Sr_{0.2}Ga_{0.83}Mg_{0.17}O_{2.815}$	[a] 800 [b] 700	—-	[a] 0.17 [b] 0.08	It shows long term stability	
$La_{0.8}Sr_{0.2}Ga_{0.85}Mg_{0.15}O_{3-\delta}$	[a] 850 [b] 800	—-	[a] 0.0782 [b] 0.0606	Fabricated by using glycine nitrate combustion method	
$La_{0.9}Sr_{0.1}Ga_{0.9}Mg_{0.1}O_{2.9}$	800	—-	0.051	Prepared by using the citrate sol-gel method and then calcined at 1400 °C	
$La_{0.9}Sr_{0.1}Ga_{0.8}Mg_{0.2}O_{3-\delta}$−2 wt.% Al_2O_3	800	10.6 (27–800 °C)	8.8	Hot isostatic-pressing (HIP) was used to fabricate the dense coating and then sintered in air-atmosphere.	[60]
$La_{0.90}Sr_{0.10}Ga_{0.76}Mg_{0.19}Co_{0.05}O_{3-\delta}$	100–1000	12.7 (27–1200 °C)	~x223C 0.30–0.39	HIP method was used to fabricate the dense coating and then sintered in air-atmosphere.	[33]
$La_{0.90}Sr_{0.10}Ga_{0.45}Al_{0.45}Mg_{0.10}O_{3-\delta}$	500	10.9 (27–950 °C)	~x223C 0.25	Citric acid combustion method is used to fabricate this powder and were sintered in air-atmosphere	[61]
$La_{0.90}Sr_{0.10}Ga_{0.76}Mg_{0.19}Fe_{0.05O3-\delta}$	100–1000	11.6 (27–1200 °C)	~x223C 0.44–0.39	Hot isostatic-pressing was used to make a compacted pellet and sintered in air-atmosphere.	[57]
$La_{0.9}Sr_{0.1}Al_{0.9}Mg_{0.1}O_{3-\delta}$	300–1000	11.2 (27–950 °C)	0.7	Powders were synthesized using a solid-state reaction method and sintered in air for 5 hrs at 1450–1500 °C.	[58]
$LaSc_{0.9}Mg_{0.1}O_{3-\delta}$	1000	—-	2.0	Calcined powder was sintered after being isostatically pressed at 200 MPa.	[62]
$La_{0.9}Sr_{0.1}InO_{3-\delta}$	200–1000	—-	1.9	The powder was isostatically pressed and calcined at 20 MPa before being cold isostatically pressed at 150 MPa.	[63]
$La_{0.9}Sr_{0.1}Sc_{0.9}Mg_{0.1}O_{3-\delta}$	300–1000	—-	2.3	The powder obtained through the solid-state reaction method was calcined and uniaxially pressed.	[64]
Bi_2O_3 and $La_2Mo_2O_9$-based electrolytes					
$La_{1.7}Bi_{0.3}Mo_2O_9$	1000	14.8 (100–350 °C)	1.4	Ball mill powder was initially pressed and then sintered in the air using a closed-alumina container.	[65]
$La_2M_{1.7}W_{0.3}O_9$	1000	14.4 (100–350 °C)	1.39	Ball mill powder initially pressed and then sintered in air using a closed-alumina container.	[66]
$(Bi_{0.95}Zr_{0.05})_{0.85}Y_{0.15}O_{1.5+\delta}$	250–800	13.8 (47–437 °C)	19.2–26.9	Hot isostatic-pressing was used to make a compacted pellet and sintered in air-atmosphere.	[67]
$Bi_2V_{0.90}Cu_{0.1}O_{5.5-\delta}$	100–750		14.1–10.6		[68]

(*continued on next page*)

Table 1 (*continued*)

Composition	Operating Temp(°C)	TEC1 × 10^6 (/K).	Conductivity (Scm^{-1})	Remarks	Ref
		18.0 (457–757 °C)		Conventional ceramic powders are pressed and sintered in air for 15–40 hrs at 900 °C.	
Other Electrolytes					
$Gd_2Ti_2O_{7\pm\delta}$	1000	10.8 (50–1000 °C)	0.44	Before sintering powder was pressed at a pressure of 200 MPa.	[69]
$La_{9.83}Si_{4.5}AlFe_{0.5}O_{26-\delta}$	1000	8.9 (100–1000 °C)	0.46	Powder was initially pressed by ball milling and then pressed it by HIP	[70]
$Gd_{1.86}Ca_{0.14}Ti_2O_{7-\delta}$	500–820	10.4 (127-1000 °C)	10.44	A typical ceramic process was used to make the powders, which were subsequently crushed and sintered in the air.	[71]
$La_7Sr_3Si_6O_{24}$	1000	9.1 (100-1000 °C)	0.51	Powders were sintered in the air between 1650 and 1500 °C for 10 hrs after being uniaxially pressed at 120–250 MPa.	[72]

ionic conductivity because its ionic radius ($r^{3+}_{Gd,\ VIII} = 1.053$) is close to r_c. Omar et al. [45] used a co-doping approach in CeO_2 to ensure the accuracy of Kim's argument, choosing the co-dopant pair, i.e., Nd^{3+} and Lu^{3+}, based on their respective ionic radius. All co-dopants were added in proportion to r_c, so that the positive elastic strain caused by the larger dopant cation (Nd^{3+}) can be remunerated by the negative elastic strain caused by the smaller dopant cation (Lu^{3+}). It, therefore, in turn, hinders any fluorite lattice distortion that is common in single-doped ceria systems. Even though the lattice elastic strain in the co-doped compositions is negligible, the ionic conductivity value is lower than that of Gd-doped CeO_2. Although the ionic radius of Y^{3+} is closer to r_c, the ionic conductivity of Y^{3+} doped CeO_2 is lower than that of Gd^{3+} and Sm^{3+}-doped CeO_2 [45].

It was proposed by Andersson et al., [46] that oxygen vacancies in Pm^{3+} doped CeO_2 have no site preferences and can coexist with both dopant and host cations. As a result, oxygen vacancy diffusion is facilitated, and ionic conductivity in this system is increased. As a result, among the rare earth trivalent cations, it was anticipated that Pm^{3+} is the best dopant for achieving higher ionic conductivity in CeO_2. But it was found that $Pm^{3+}$is a radioactive element so it is not possible to use it for SOFC electrolyte applications. Due to this reason, a co-doping scheme with Nd^{3+} and Sm^{3+} as co-dopants was suggested for CeO_2. There are numerous reviews and articles in the literature that provide a detailed account of the co-doping and doping materials that have been tested so far. Table. 1 summarize some of the most commonly used co-doping and doping materials.

3. Recent advancement in electrolyte materials

The electrolyte placed between a porous anode and cathode is responsible for performing a vital function of separating the anode and cathode gasses. To do it efficiently, the electrolyte's compactness is a crucial factor. Moreover, the ionic conduction inside electrolyte is a significant phenomenon partially defining the SOFC's performance. Based on the species being transferred, the SOFCs are divided into two main categories including oxygen ion-conducting SOFC and proton-conducting SOFC. As the activation energy associated with proton diffusion is lower than that of oxygen diffusion, it is easier to obtain higher activity in the prior one. Dual ion-conducting SOFC is another category that has gained enormous attention in recent years. In this SOFC, the electrolyte simultaneously diffuses oxygen as well as proton ions. The reaction mechanisms in each type of SOFC are different because of different mechanisms of ion conduction [73]. This section gives a comprehensive review of electrolyte materials. Various parameters affect the properties of these materials including grain boundary structure, dopant type, and impurities [74]. However, this discussion is out of the scope here.

3.1. Zirconia-based electrolytes

The oxygen ions are diffused from the cathode to the anode in oxygen ion-conducting SOFCs (O-SOFCs) using a suitable electrolyte. To obtain an enhanced output of the cell at the working temperature, electrolytes should exhibit a higher ionic conducting along with good mechanical and chemical stability. The ionic conductivity in a solid material is driven by the concentration gradient and mainly depends on the lattice defects. There have been numerous reported studies in the literature covering a wider range of materials being considered as an electrolyte for SOFC [75]. In the 1990s only limited studies were performed corresponding to developmental strategies for lanthanum gallate materials (Sr- and Mg-doped lanthanum gallate, LSGM) and newly developed electrolytes with oxygen ion conductivity and other parameters being imperative for further advancement in SOFC. Studies suggested that newly introduced materials were not compatible to constitute any breakthrough similar to LT-SOFCs.

Yttria-stabilized zirconia (YSZ) is a typical electrolyte material with excellent chemical stability in both reducing and oxidizing atmospheres because of the tetrahedral anionic site and cubic cationic arrangement, it provides numerous vacancies in the route of oxygen ion transfer [76]. Pure zirconia is not stable at higher temperatures, so to stabilize it dopants such as calcium oxide and magnesium oxide are used. The resultant YSZ electrolytes are capable of operating at a temperature above 850 °C. However, the optimum temperature value is around 700 °C to lower the manufacturing cost and to increase the output [77]. The operating temperature can be reduced either by minimizing the electrolyte thickness or by implying electrolytes with higher ion conduction. Pure zirconia is available in three crystal structures including monoclinic, tetragonal, and cubic [78]. The thermal stability becomes poor in the process of transforming its crystalline structure. The partial divalent or trivalent cationic substitution results in cubic structure stabilization and better oxygen conductivity due to the availability of more vacancies within the oxide lattice. The ionic conductivity reduces as the operating temperature decreases, this is why when YSZ is used as an electrolyte the membrane should be capable of withstanding lower ohmic resistance [79]. In case of trivalent ions, the doping effect is observed to be in the increasing order of Sc > Yb > Er >Y > Dy > Dd > Eu [80]. The scandium oxide-stabilized zirconia (ScSZ) has exhibited the highest conductivity reported to be as high as 0.003 Scm^{-1} at 500 °C [81]. The thin layer ScSZ electrolytes have shown improved output at intermediate ambient temperatures when coupled with suitable electrodes [82–84]. As compared to scandium oxide, the material cost of erbium oxide and ytterbium oxide is less and their respective ionic conductivity values are in an acceptable range. Therefore, the zirconia stabilized by Er or Yb have more potential to be applied in SOFCs at a lower temperature.

However, the limited choices of cathode material are the major bottleneck regarding the implementation of stabilized zirconia electrolytes. It is reported that cathodes made up of barium, lanthanum, etc. can easily react with YSZ, resulting in an enormous increase in ohmic as well as polarization resistance which causes lower cell shelf life [85,86]. It is reported in the literature that dopped cerium oxide materials possess higher ionic conductivity as compared to stabilized zirconia.

However, a significant variation is observed in the values. The addition of alumina oxide and zinc oxide is proven to be an effective method for sintering performance improvement [87,88]. Another major issue is impurities present in the electrolytes such as silicon oxide. Silica deposits itself at the boundaries of electrolytes, causing resistance in oxygen ion conduction. Therefore, the purity of electrolytes during the preparation phase should be controlled strictly.

Several zirconia dopants have been studied, and just one, ScSZ, produces significantly greater conductivity than YSZ due to the nearly perfect size match between Zr and Sc cations. At intermediate temperature conditions, the scandia metastable zirconia has shown very high conductivity. It is reported in the literature that the conductivity of YSZ electrolyte (at a temperature of 1000 °C) was equal to that of ScSZ electrolyte (at a temperature of 780 °C) [89]. Moreover, the ScSZ has the same mechanical properties as that of YSZ, however, due to higher associated costs, commercialization was not pursued. The doping of Sc is frequently used in parallel with any second dopant i.e., Ce [14] and Bi [15]. Bi also acts as a sintering aid, resulting in a decrease of sintering temperature which in turn enhances the zirconia grains growth [21].

3.2. Ceria-based electrolytes

Several review articles are published in which the singly-doped ceria properties are discussed. In literature, among various dopants, the Sm or Gd has been reported to be giving the highest yield. In few cases, the multi-dopant ceria is reported to have better total and grain boundary conductivity than the singly-doped ceria. Gadolinium oxide doped CeO_2 (GDC) and samarium oxide doped CeO_2 (SDC) are alternate electrolyte materials which can be used even at higher oxygen partial, pressures in LT-SOFCs [18,50]. The conductivities are reported to be 6.1×10^{-2} Scm^{-1} and 6.7×10^{-2} Scm^{-1} for SDC and GDC respectively at an operating temperature of 750 °C. Whereas, at temperature values less than 600 °C, GDC showed a higher ion conductivity than SCSZ and YSZ. However, at lower oxygen partial pressures or higher temperatures, the SDC and GDC electrolytes reduced Ce^{+4} to Ce^{+3}. Because of this reason, the electrolytes based on cerium materials conduct current which in turn decreases the cell's OCV, resulting in lesser efficiency. A thin YSZ layer applied in between the anode layer and electrolyte can help to cope up with this issue. However, the inter-diffusion between YSZ electrolyte and cerium oxide is still a challenge.

3.3. $LaGaO_3$-based perovskite electrolyte

Lanthanum or alkaline earth metal (A) and transition metal (B) element altogether make ABO_3- type perovskite structure. Most of the perovskite cathode materials exhibit both electronic and ionic conductivity in SOFCs. Some of the materials including $La_2Mo_2O_9$, doped $LaGaO_3$ perovskites, brownmillerite-like phases ($A_2B_2O_5$), and $LnBO_3$ (B = Sc, In, Al, Y) perovskites, which are related to perovskites have also shown quite high oxygen ion conductivity at IT-temperature, which makes them suitable for use as an electrolyte in SOFCs. The most researched perovskites for IT-SOFCs among the stated ones are $LaGaO_3$ [90].

Variable oxygen vacancies can be created by doping the A site of $LaGaO_3$ with divalent alkaline earth metals (Ca^{2+}, $Sr^{2+,}$ and Ba^{2+}). In addition, partial replacement of La^{3+} by Sr^{2+} resulted in the maximum ionic conductivity because Sr^{2+}has the closest ionic radius to La^{3+}, theoretically speaking, the reason behind this increase in conductivity is the creation of more oxygen vacancies by this substitution. However, practically this increase has certain limitations which include the creation of impurities such as $SrGaO_3$ or La_4SrO_7 when we substitute Sr^{2+} more than 10% of the pure perovskites and it ultimately affects negatively on ionic conductivity. The B-site of $LaGaO_3$ can be doped with divalent ions to increase oxygen vacancies. If B-site would be doped with Mg^{2+}, it will significantly improve the ionic conductivity of the electrolyte. Doping limitations of La^{2+}on the A-site that could be because of an enlarged crystal lattice can be increased by the addition of Ga^{3+} with Mg^{2+} on the B-site [29].

$La_{0.9}Sr_{0.1}Ga_{0.8}Mg_{0.2}O_{2.85}$ (LSGM) is the most common oxygen-ion-conducting electrolyte, which was reported almost simultaneously by two different groups in the United States and Japan respectively. It exhibits a pure O_2 ion conductivity with high thermal chemical stability. It has an excellent conductivity of 1.54×10^{-2} Scm^{-1} at 595 °C, making it suitable for IT-SOFC electrolytes [56]. Pelosato et al., sintered LSGM in an aqueous medium by a co-precipitation method, and the sintered sample had a relative density and total conductivity of 98% of 1.13×10^{-2} Scm^{-1} at 600 °C, respectively [57]. The partial replacement of Sr^{2+} with La^{3+} and doping of Mg^{2+} into the gallium sub-lattice increase its oxygen vacancy concentration (V_O). However, NiO reacts with LSGM to form $LaNiO_3$ during the manufacturing process, which is not a conductive layer between the electrolyte and anode. This problem can be evaded by deposing a thin layer of GDC between the electrode material and the electrolyte. However, one of LSGM's drawbacks is its low sinterability. Therefore, the attainment of dense LSGM electrolytes is a significant problem. While the sintering of anode material would lead to improved LSGM electrolyte densification, but it causes negative effects on mechanical strength and its conductivity. The ionic conductivity and sinterability of LSGM can be enhanced by using the route of doping. Researchers reported Co and Fe as dopants to enhance the density and ionic conductivity of LSGM electrolyte [58] further researchers focused on the development of cost-effective dopant materials including Al, Sc, and In as biased substituents of Ga in $LaGaO_3$. Reported results were found to be acceptable with the remarkable influence of microstructural effects in the origination of grain boundaries responsible for the blockage of ions. Ni- doping on the B-site of LSGM proved to be an excellent way for the enhancement of electrochemical performance without affecting the conductivity. However, Ni dissolution is a major problem during cell sintering at high temperatures [59]. Furthermore, insufficient content of La in electrodes gives rise to the origination of non-perovskite phases. Various strategies were proposed and studied for the development of SOFCs with thin LSGM electrolytes comprehend to LSGM/doped ceria layered electrolytes in which ceria serve as a blockade to diffusion [33].

3.4. $BaZrO_3$ and $baceo_3$-based electrolytes

In literature there are three basic requirements for a compatible electrolyte material and these requirements are listed as, enhanced sinterability, higher ionic conductivity, and strong chemical stability. $BaCeO_3$-based electrolytes exhibit higher values (0.01 Scm^{-1}) of proton conductivities and stabilities than inorganic proton conductors. Due to these properties doped $BaCeO_3$ materials are considered as most commonly used proton conductors [91]. Matsumoto et al. studied the effects of several dopants on the stability and conductivity of $BaCeO_3$, including Sc^{3+}, Y^{3+}, Lu^{3+}, Yb^{3+}, $In^{3+}$and Tm^{3+} [62]. It was reported that ionic conductivity increases but chemical stability decreased with the increased ionic radius of dopants. Comparative studies reveal that best conductivity was reported for the Y^{3+}-doped $BaCeO_3$ (BCY) material and Sc^{3+}-doped $BaCeO_3$ were characterized as the most stable oxides among all which have been studied so far.

According to Kröger-Vink notation equation, 16 represents the substitution of trivalent cations (m-dopant) at B- sites for Ce^{4+} ions [64].

$$2Ce_{ce}^{x} + O_o^x + M_2O_3 \rightarrow 2M_{ce}^{'} + V_o^{\cdot\cdot} + 2CeO_2 \quad (16)$$

It has been found that proton conductivity is dependent upon two important parameters including the concentration of oxygen vacancies which is responsible for the origination of reactive site to facilitate the ionic diffusion. Protons align in perovskite materials when exposed to hydrogen-rich or water vapor atmospheres, resulting in proton deficiency $(OHO)^o$ and reduced oxygen ions, as illustrated in the Eq. (17).

$$H_2O + O_o^x + V_o^{\cdot\cdot} \leftrightarrow 2OH_o^o \quad (17)$$

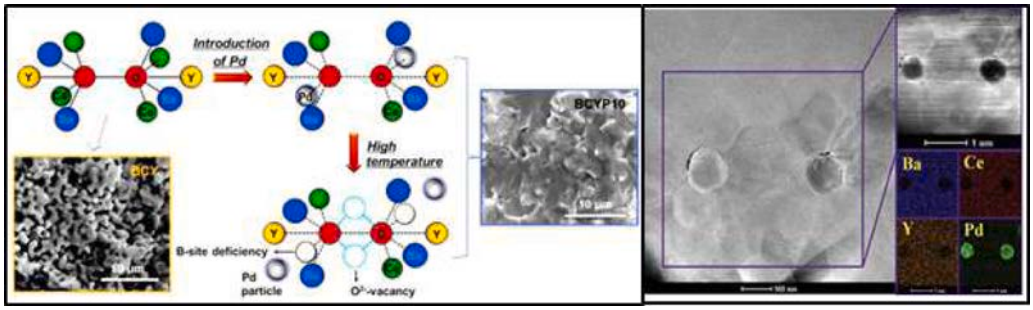

Fig. 3. Schematic for the mechanism of enhanced sintering of BCY electrolyte after Pd incorporation. STEM and EDX elemental distribution of several elements (Pd, Ce, Ba, and Y) in BCYP10 pellets sintered at 1400 °C. [93] are illustrated on the right side.

Low proton conductivities are measured due to stable cubic structure thus, conductivity can be enhanced by defect formation into the structure. Defect formation is influenced by the size and atmosphere of dopants. Eq. (18) represents the substation by higher size ionic dopant like Sm^{3+} into A-site (Ba^{2+})

$$2Ba^{x}_{Ba} + M_2O_3 + V^{\cdot\cdot}_{o} \rightarrow O^{x}_{o} + 2M^{o}_{Ba} + 2BaO \quad (18)$$

Eq. (15) indicates the reaction corresponds to the consumption of oxygen instead of the production of oxygen vacancies results in lower proton conductivity [92]. According to reported studies phenomenon of doping and co-doping help to improve the following parameters of SOFCs as given below,

1 Proton conductivity.
2 Stability of $BaZrO_3$ and $BaCeO_3$ as a result of their perovskite structure.

Liu et al., [93] improved the performance of BCY by designing new proton-conducting perovskite with the composition of $BaCe_{0.8}Y_{0.1}Pd_{0.1}O_{3-\delta}$ (BCYP10) adopting the Pd ingress-egress approach as illustrated in Fig. 3. In this approach, a sufficient amount of Pd was introduced that results in increased ionic conductivity. Therefore, SOFC with a BCYP10 electrolyte has been reported for delivering a high value of PPD (645 $mWcm^{-2}$ at 700 °C). Liu et al., studied the doping effects of Al^{3+} doping into $BaCeO_3$ to investigate the properties related to chemical stability and conductivity [93,94]. Their studies revealed that doping of Al into $BaCeO_3$ provides enhanced chemical stability as compared to doping of rare earth metal cations. Bi et al., reported the formation of $BaCe_{0.7}Ta_{0.1}Y_{0.2}O_{3-\delta}$, through co-doping of Ta and Y into the Ce site of $BaCeO_3$ and revealed that co-doping provides acceptable chemical stability against Carbon dioxide and water. Shao and Tadé [17] worked on developing and designing several exsolution strategies for the development of nano-particles to assist the enhanced sinterability of proton-conducting electrolytes. They performed the doping at higher operating temperatures by incorporating Pb-based nanoparticles into the perovskite structure. Fig. 3 demonstrate covering of BCY grain-boundary and thermal reduction of Pb nanoparticles thus, allowing the sintering of electrolyte membrane at reduced operating temperature. Due to increased sintering aid and amended grain boundaries resulted in electrolyte showed considerable conductivity. Iwahara et al., [95] reported the synthesis of Nd-doped $BaCeO_3$ ceramic electrolyte manifesting mixed conduction by oxide ions and protons. Reported studies suggest that the thickness of electrolyte film is greatly influenced by ohmic resistance so, strategies should be developed to lessen the effect of ohmic resistance for the promotion of OCV (open-circuit voltage) which plays a remarkable role in the determination of cell performance of solid oxide fuel cells. However, experimental data suggest that Nickel should be considered as, promising anode material capable to substitute other materials except for platinum for the Nd-doped $BaCeO_3$ electrolytes.

The effects of titanium doping on the stability and conductivity of $BaCe_{0.8-x}Ti_xY_{0.2}O_3$- investigated by Medvedev et al. [96,97]. Owing to the highly electronegative character of titanium exhibit remarkable stability in CO_2-supporting atmospheres. In addition, an issue was encountered related to low protonic conductivity owing to decreased transport of protons in Ti-doped ceramics. Pasierb et al. [98] reported the effects of incorporation of yttrium on barium cerate, comprising of sufficient amount of titanium. By specifying particular reaction parameters of heating (1200 °C for 24 h) and sintering (1600 °C for 24 h), the solid-state reaction method was used to synthesize Ba $(Ce_{0.95}Ti_{0.05})_{1-x}Y_xO_{3-\delta}$ material. It has been observed that conductivity of these materials was increased in both environments i.e., in reducing (5 vol% H_2 + 95 vol% Ar) and oxidizing (21 vol% O_2 + 79 vol% N_2) with increased concentration of yttrium. Zhang et al., [147] further extended their studies related to co-doping of $BaCe_{0.8-x}Sm_{0.2}In_xO_{3-\delta}$ materials but their experimental data revealed that conductivity was decreased with an increased amount of indium. Su et al., [99] reported a relatively new method for investigating fluorine effects in barium cerate by utilizing powder forms of F-doped $BaCe_{0.8}Sm_{0.2}O_{3-\delta}$ and studies to suggest that stability of these materials under CO_2 atmosphere can be explained in terms of reduced basicity of $BaCeO_3$ correspond to enhanced chemical stability in acidic gasses without any loss in conductivity by the implementation of F^- as a dopant. However, more research is needed to determine the impact of these composites on electrolyte characteristics. To improve the sinterability of BZY, sintering aid is commonly used [68]. As stated above, doping is usually carried out to originate the oxygen vacancies within the lattice to promote the protonic conductivity of oxide ions [100]. Studies suggest that sintering properties can be improved by the application or effect of dopant [101]. Guo et al., extended their research to investigate the doping effects of Zr on the performance of $BaZr_yCe_{0.8-y}Y_{0.2}O_{3-\delta}$ ($0.0 \leq y \leq 0.8$) for P-SOFCs [102] and considering several parameters they reported that thin-film electrolyte sintering does not support by anode-based cell configuration and by considering several properties as, stability, sinterability electrochemical activity of $BaZryCe_{0.8-y}Y_{0.2}O_{3-\delta}$ they manipulated that (BZCY0.4) is considered promising electrolyte for P-SOFCs. Fabbri et al., reported a newly develop proton conductor through partial substitution of Zr ions with Pr-ions, i.e., $BaZr_{0.7}Pr_{0.1}Y_{0.2}O_{3-\delta}$ (BZPY) [103] and supported their work by reporting chemical stability and higher protonic conductivities (2×10^{-2} Scm^{-1} at 600 °C) under wet air-supported atmosphere and in addition to this they reported improved sinterability in comparison with BZY. Sun et al., [121] studied the doping of Sn (10 mol %) to B-site of BZY for the formation of $BaZr_{0.7}Sn_{0.1}Y_{0.2}O_{3-\delta}$ (BZSY) and highlighted their improved values of conductivities (1.6×10^{-3} Scm^{-1} at 600 °C) in H_2 supporting atmosphere comprising of 3% H_2O with adequate chemical stability. Cell corresponding to the following configuration of anode and cathode Ni + BZSY | BZSY (12 μm thickness) | $Sm_{0.5}Sr_{0.5}CoO_{3-\delta}$ + SDC respectively provided a PPD of 360 mW cm^{-2} at 700 °C. Liu et al. contributed to the discovery of a $BaZr_{0.7}Nd_{0.1}Y_{0.2}O_{3-\delta}$ (BZNY) with improved proton conductivity, sinterability for BZY [104].

Considering the small size of protons, their activation energy was

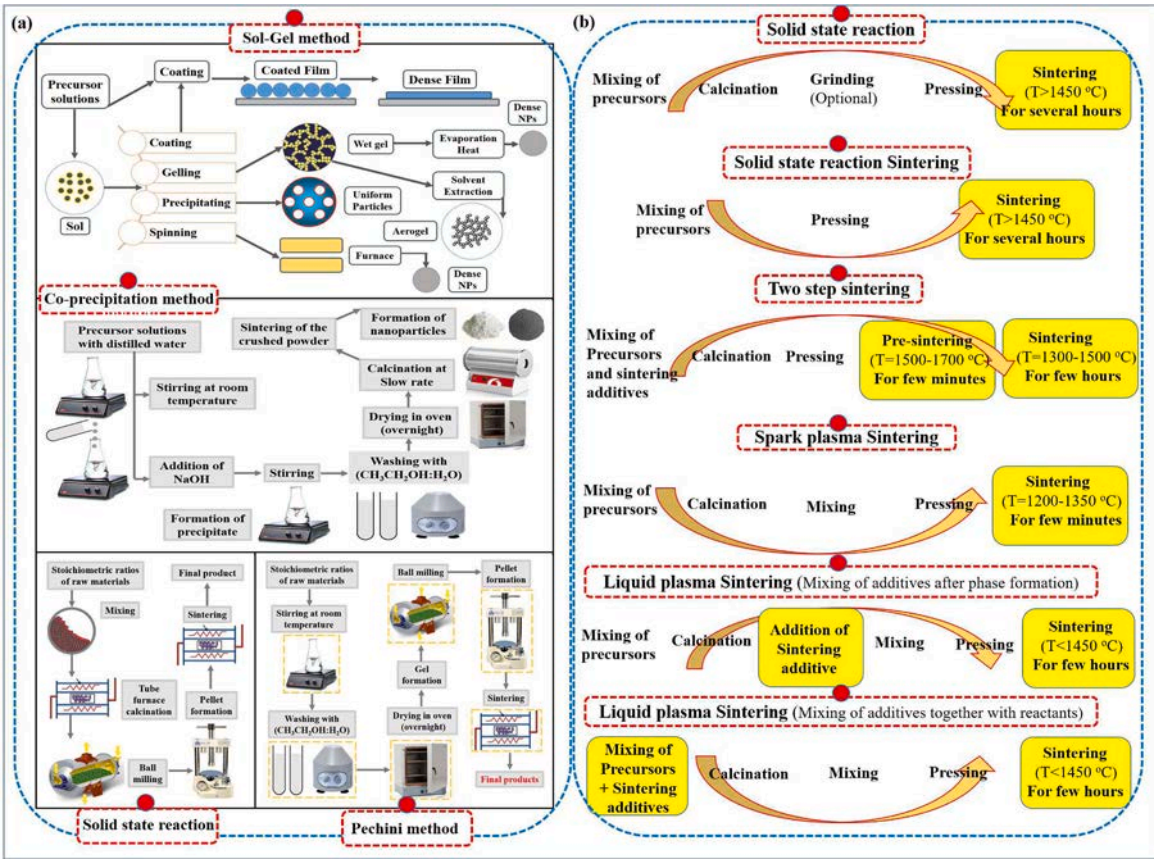

Fig. 4. Schematic diagram for the synthesis routes labeled as (a). sol-gel method, (b). co-precipitation route, (c). solid-state reaction route, (d). pechini method and (e). the various sintering routes are depicted in a flowchart.

lesser than that of O_2 ions. Therefore, proton conductive perovskites such as $BaZr_{0.1}Ce_{0.7}Y_{0.2}O_{3-\delta}$ (BZCY), $BaCeO_3$, and $BaZr_{0.1}Ce_{0.7}Y_{0.2-x}Yb_xO_{3-\delta}$ (BZCYYb) have been recent, achieved more appeal from new electrolytes. SOFC's working temperature can be reduced to below 500 °C. It operates at a temperature range of 300–500 °C, which gives rise to significant benefits, such as fast startup/shutdown, increased lifespan, and flexible sealing. $SrCe_{0.8}Y_{0.2}O_3$ (SCY) and $BaCe_{0.8}Y_{0.2}O_3$ (BCY) are the two most prevalent perovskites with higher proton-conductivity. Their conductivities are comparable to high oxygen ion-conducting electrolytes (for example, LSGM and doped ceria). One of the drawbacks of these two materials is their poor stability in CO_2 and H_2O vapor atmosphere respectively [29].

$BaZr_{0.8}Y_{0.2}O_3$ (BZY) is a proton-conducting perovskite with higher ionic conductivity than SCY and BCY electrolytes, even it is highly stable under CO_2 and H_2O vapor atmosphere. However, the BZY electrolyte's poor sinterability affects the oxide ion conductivity. Sintering aids were widely used to enhance BZY electrolyte sintering. The grain-boundaries get wet due to sintering aids and to indorse sintering [105]. The use of appropriate sintering aids can attain higher densification effects at lower operating temperatures. Whereas in some cases, the output performance of the cell does not exhibit obvious changes under O_2 containing SOFC's. The main reasons for the adverse effects of sintering aids on BZY are proton transport and lack of appropriate cathode materials. Ryan and Tong, studied an effective production of a $BaCe_{0.7}Zr_{0.1}Y_{0.1}Yb_{0.1}O_3$ (BCZYY) electrolyte for SOFC applications. They used $BaCo_{0.4}Fe_{0.4}Zr_{0.1}Y_{0.1}O_3$ (BCFZY) as a cathode material with 1 wt%-NiO as a sintering aid, which accomplished a peak power density of 455 $mWcm^{-2}$ at 500 °C respectively, which consequence a substantial development to attain an intermediate range of operating temperatures for SOFCs. Whereas, Yang et al., suggested a popular dual nature ion-conducting electrolyte $BaZr_{0.1}Ce_{0.7}Y_{0.1}Yb_{0.1}O_{3-\delta}$ (BZCYYb) with enhanced ionic mobility and considerable sinterability [106], and duality of the reported electrode was further approved by Zhou et al., [107].

3.5. Bismuth-based electrolytes

Bismuth oxide was found to be having the highest conductivity and stability among several electrolytes. However, it was only stable in a certain temperature range (730 °C to 804 °C), whereas, it was reduced into bismuth metal at lower oxygen pressure. Thus, its use as an electrolyte is still hindered in SOFCs application. Doping of Er[54], La[20], Y[23], and Sr[55]can stabilize the beta bismuth oxide cubic structure. Another closely related family is BiM-VO_x which showed conductivity and stability characteristics similar to that of bismuth oxides. For instance, $Bi_2V_{0.9}Cu_{0.1}O_{5.35}$ is reported to have 0.1 Scm^{-1} conductivity at a temperature of 600 °C [24].

3.6. Other electrolytes

A Limited number of promising materials have been discussed here. Lanthanum silicate $La_{9.33+x}Si_6O_{26+1.5x}$ manifests significant conductivity that can be enhanced by the addition of dopants (Al and Mg) [108]. Various SOFCs have been introduced with relatively lower values of power densities (0.166 Wcm^{-2} at 600 °C) [109]. Germanium-containing analogs, $La_{10y}Ge_6O_{26-\delta}$ were studied for their remarkable conductive behavior but these materials were failed in compatibility with electrode materials and in redox cycling [110]. Melilite structure $La_{1.54}Sr_{0.46}Ga_3O_{7.27}$ have been investigated for their enhanced values of conductivities over a wide range of temperature (600–900 °C). In addition to these materials, several studies have been reported for $Na_{0.5}Bi_{0.49}Ti_{0.98}Mg_{0.02}O_{2.96571}$ which provide remarkable oxygen ion conductivity related to Gd doped ceria (GDC). Another material ($Sr_{1-x}Na_xSiO_{30.5x}$) has

been reported with comparable conductivity with GDC although other reported groups were failed to procreate results [111].

3.7. Comparison between different synthesis routes

Different synthesis techniques have been used to prepare different perovskite materials. Here we discussed a few of them: sol-gel method, co-precipitation route, pechini method, and solid-state reaction route. Some of the sintering methods with and without using sintering additives include solid-state reactive sintering (SSRS), solid-state sintering (SSS), spark plasma sintering (SPS), and two-step sintering (TSS), liquid phase sintering (LPS) respectively. Each of these techniques has its pros and cons. The main differences contain on phase purity, sintering temperature and time, due to sintering and phase formation in a single step. Different synthesis techniques have been used to prepare different perovskite materials.

a Sol-gel method

The sol-gel method is highly applicable in material science for the production of solid materials from small molecules as precursors. Different types of metal oxides (as active material) which are used for multiple applications in energy storage devices can be easily synthesized by using the sol-gel route. The term "sol" refers to a colloidal solution, the initial product of the sol-gel route which is then further transformed into a diphasic system. The diphasic system represents both liquid and solid phases which exhibit diversity in morphological behavior from distinct particles to an incessant polymer network. Different methods are used in the case of colloid, to enhance the gel-like properties by the removal of a substantial amount of liquid that results in increased particle fraction or density. Sedimentation is the simplest method for increasing the particle fraction. Phase separation can be accelerated by using centrifugation. Complete removal of residual fluid (solvent) requires a drying process, which is accompanied by a significant amount of shrinkage and densification. Gel-porosity is an important parameter for the determination of the rate at which residual solvent or liquid is removed. During phase processing, the microstructure of the desired material is significantly influenced by changes that are enforced for structural modeling. A firing process or thermal treatment is compulsory to implement which favors grain growth, poly-condensation, and densification which are important parameters for enhancing mechanical and structural properties. Densification is accomplished at a considerably low temperature, which distinguishes it from other processing approaches and makes it more favorable for phase processing. By using dipping or spin coating a film can be designed by the deposition of precursor sol to a substrate, that further cast into an appropriate container to attain anticipated shapes e.g., monolithic ceramics, glasses, fibers, membranes, aerogels or can be converted into powder as micro and nano-spheres. The sol-gel method is an adequate technique to control the chemical composition of desired product, operating at low temperatures. The sol-gel method is applied for the complete introduction of very minute amounts of dopants, including organic dyes and rare earth elements in the sol and their constant spreading in the desired product. Materials or products which are fabricated through the sol-gel method have been extensively used in several fields such as in separation techniques e.g., energy, chromatography in optics, (bio) sensors, space, medicine (such as controlled drug release), electronics, and reactive material [116]. Fig. 4(a) shows the schematic mechanism for the sol-gel method.

a Co-precipitation route

Co-precipitation is a method that depends upon the solubility of substances, it involves the precipitation of materials that are soluble under normal conditions. In many cases for chemical analyses co-precipitation is regarded as a problem for obtaining undesirable products e.g., in gravimetric analysis co-precipitation is the main problem as it causes the precipitation of impurities within the analyte that results in an increased mass of the analyte. The gravimetric analysis deals with the determination of purity of a sample or analyte by measuring its mass and increased mass due to precipitation of impurities affects the results of gravimetric analysis. This problem can be overcome by treating the analyte through redissolving or digestion. Co-precipitation can occur in three different ways through adsorption, occlusion, and inclusion. Inclusion involves the crystallographic defect, that arises because in the similarity between ionic radius and charge of impurity and analyte, impurity lodges a lattice site in the crystal structure. Impurity is often regarded as adsorbate that gets adsorbed on the surface of the precipitate. However, this method is also used to produce desirable active materials for energy storage devices e.g., metal oxides can be produced by using the co-precipitation method. Co-precipitation is widely applicable in radiochemistry, chemical analyses as well as potentially towards many environmental concerns that involve comprising acid mine drainage, water resources, transportation of metal pollutants at industrial and defense sites, fouled waste repositories migration of radionuclide, wastewater treatment technology, and metal constituents in an aquatic system [119]. Fig. 4(b) shows the schematic mechanism for the co-precipitation route.

a Solid-state reaction route

The solid-state reaction route is the most reported and convenient method that utilizes a mixture of solid as a preliminary material for the preparation of polycrystalline solids. Solids are usually non-reactive under room temperature and require specific reaction conditions. Therefore, for a reaction to occur at an appropriate rate solid materials/reactant are heated at higher temperatures 1000 to 1500 °C and homogenized through grinding. The number of crystallites is increased by the formation of pellets through the hydraulic press. Different parameters including structural properties of preliminary materials, the surface area of solids, and reaction conditions determine the reaction rate and feasibility of solid-state materials. The rate of reaction is very slow that, it acquires hours, days, or sometimes weeks with intermediate grinding for the completion of the reaction [122]. Fig. 4(c) shows the schematic mechanism for solid state reaction route.

a Pechini method

Pechini method is a contrarily polymerizable complex process. The liquid-mix technique involves the formation of extremely uniform and finely dispersed material oxide as well as complexes and producing an intermediate of polymer gel. This procedure was suggested in 1967 as a technique; for the manufacturing of capacitors, dielectric film of niobate, and titanates of alkaline-earth and lead elements were deposited. Afterward, the method was altered for in-lab production of highly dispersed multicomponent oxide materials. This process involves a thorough mixing of positive ions in solution, removal of the polymer matrix, and development of an oxide precursor with a greater degree of homogeneity and controlled conversion of solution into polymer gel. It involves the introduction of metal salts or alkoxides into citric acid solution with ethylene glycol. Citric complexes assist the enhanced dissemination of ions and inhibit the further separation of ions during later stages of the process and complex formation controls the distinct behavior of ions present in the solution. Polymer citrate gel formation is processed through poly-condensation of citric acid and ethylene glycol above 100°C. Above 400°C polymer matrix instigate to oxidation and pyrolysis that results in the production of X-ray amorphous oxide and/or carbonate precursor desired homogenized and dispersed material can be obtained by subjecting the precursor to further heating. A variety of materials such as fluorescent, dielectric, high-temperature superconductors, catalysts, and magnetic materials are being synthesized by using pechini method, further, it can be used for oxide film deposition

Table. 2
List of some novel ionic and proton-conducting electrolytes with their ohmic resistance (R_Ω), polarization resistance (Rp), conductivity (Scm^{-1}), and peak power density ($mWcm^{-2}$) respectively at different processing temperatures.

Sr. No	Electrolytes	Synthesis route	Anode	Conductivity (S cm^{-1}) / Temp (°C)	PPD ($mWcm^{-2}$)/ Temp (°C)	$R_\Omega(\Omega cm^2)$	Sintering temp(°C)	Fuel	Ref
1	$La_{0.995}Sr_{0.005}NbO_4$ (LSN)	Spray-pyrolysis	Ni- LSN	—	1.35 (800 °C)	23 (800 °C)	1450	—	[112]
2	$La_{0.99}Ca_{0.01}NbO_4$ (LCN)	—	Ni-LDC	—	65 (800 °C)	2.35 (800 °C)	—	—	[113]
3	$La_{0.9}Ca_{0.1}Ga_{0.8}Mg_{0.2}O_{3-\delta}$ (LCGM)	Glycine-nitrate synthesis method	Ag-Pd	—	—-	—	1400–1500	—	[114]
4	$La_{0.9}Sr_{0.1}Ga_{0.8}Mg_{0.2}O_{3-\delta}$ (LSGM)	Micro-emulsion	Ag-Pd	—	—	—	1400	—	[115]
5	$La_{1.95}Ca_{0.05}Zr_2O_{7-\delta}$ (LCZO)	Sol-gel method	Ag-Pd	—	—	—	1500	—	[116]
6	$La_{0.9}Ba_{0.1}Ga_{1-x}Mg_xO_{3-\alpha}$ (LBGM)	Micro-emulsion	Ag-Pd	4.68×10^{-2} (800 °C)	—	—	1350 to 1430	—	[117]
7	$Ce_{0.8}Sm_{0.2}O_{1.9}$ (SDC)	Modified glycine-nitrate process	Ni–SSC	—	191.8 (600 °C)	—	1400	H_2	[72]
8	$BaCe_{0.9}Sm_{0.1}O_{3-\delta}$ (BCS)	Glycine-nitrate process	NiO–BCSO	0.00938 (700 °C)	340 (700 °C)	0.689 (700 °C)	1350	(3% H_2O) H_2	[118]
9	$BaCe_{0.8}Gd_{0.2}O_{3-\delta}$ (BCG)	Conventional solid-state synthesis	Pt	—	25 (700 °C)	—	1350	H_2 or NH_3	[119]
10 1	$BaCe_{0.8}Gd_{0.2}O_{3-\delta}$ (BCGO)	EDTA–citrate complexing method	Ni-CGO		147 (600 °C)	—	1450	H_2	[114]
11	$BaZr_{0.8}Y_{0.2}O_{3-\delta}$ (BZY20)	Citric acid-nitrate gel combustion	Ni-BZY20	—	170 (700 °C)	1.4	1400	H_2 (~x223C 3% H_2O)	[120]
12	BZY/In	Citric acid-nitrate gel combustion	Ni-BZY20	—	169	0.88	1450	H_2 (~x223C 3% H_2O)	[32]
13	$BaZr_{0.8}Y_{0.2}O_{3-\delta}$-Li (BZY20-Li)	Sol-gel combustion method	Ni-BZY20	4.45×10^{-3} (700 °C) in wet Ar	53 (700 °C)	0.95 (700 °C)	1500	Wet-air, wet-Ar, wet Ar-10% H_2	[121]
14	$BaZr_{0.7}Pr_{0.1}Y_{0.2}O_{3-\delta}$ (BZPY10)	Combustion synthesis procedure	Ni-BZY20	10^{-2} (600 °C)	81	1.33 (600 °C)	1500	Wet air and H_2	[30]
15	$BaCe_{0.7}Ta_{0.1}Y_{0.2}O_{3-\delta}$ (BCTY)	Pechini method	Ni- BCTY	2.3×10^{-3} (600 °C)	195 (700 °C)	1.08 (600 °C)	1450	H_2 (~x223C 3% H_2O)	[31]
16	$BaCe_{0.7}Nb_{0.1}Sm_{0.2}O_{3-\delta}$ (BCNS)	Solid-state reaction method	Ni- BCNS	0.0026 (700 °C)	245 (700 °C)	0.31 Ω cm^2 at 700 °C	1550	Wet H_2	[122]
17	$Ba_3Ca_{0.9}Nd_{0.28}Nb_{1.82}O_{9-\delta}$ (BCNN)	EDTA-citrate complexing	Ag-Pd	—	—	—	1300	—	[123]
18	$BaZr_{0.1}Ce_{0.7}Y_{0.2}O_{3-\delta}$ (BZCY)	EDTA-citrate complexing	Ni–BZCY,	—	420 (700 °C)	0.28 (600 °C)	1450	H_2	[124]
19	$BaCe_{1-x}Ca_xO_{3-}\alpha$ (BCC)	Micro-emulsion route.	—	7.64×10^{-4} (600 °C)	—	—	1500	H_2	[125]

and coatings. Pechini method has significant importance due to its simpler path, independency towards reaction conditions (reaction not affected by the chemistry of cations present in the desired product), low-temperature treatment of precursor favor the completion of reaction depriving of sintering that results in the formation of refractory oxides in the form of nano-crystal powders. The method is limited due to the use of toxic chemicals i.e., ethylene glycol and organic reagents in excess amount as per unit of desired product's mass. Stable citric complexes are not formed in case of some elements including bismuth, silicon, etc. pyrolysis of polymer gel leads towards the fractional or thorough restoration of one of the components of polymer gel e.g., zinc, copper, ruthenium, lead, etc.) [118]. Fig. 4(d) shows the schematic mechanism for pechini method.

In this review, we will give a brief overview of the synthesis and sintering routes for preparing electrolytes as shown in Fig. 4 (a–e). Whereas, Table 2 shows some good ionic and proton-conducting electrolytes with their ohmic resistance (R_Ω), polarization resistance (Rp), conductivity (Scm^{-1}), and peak power density ($mWcm^{-2}$) respectively at different processing temperatures. However, depending on numerous aspects such as gas component materials and input purity utilized in the stack/system, SOFC cells might suffer significant performance loss in practical situations [14]. Sulfur is the most common fuel contaminant in many commercial fuels, and the poisoning effects of sulfur on the Ni/YSZ anode are well-known [15]. Silicon impurities in the fuel (resulting from silica-containing insulations or stack glass sealants) have also been demonstrated to poison the Ni/YSZ anode [16]. Significant concentrations of H_2O or CO_2 in the air can degrade cell performance on the cathode side [17]. Chromium poisoning can cause cell performance to degrade over time when cells are in touch with the metallic interconnects. Chromium in the metallic interconnect can move to cathode reactive sites and interact with the cathode, poisoning the electrode, resulting in a gradual increase in cathode polarization. To minimize chromium transport, the most frequent mitigation strategy is to apply conductive coatings (e.g., Co-Mn spinel) on the metallic connection [18–20].

4. Alternative perovskites applications in energy storage

Inorganic perovskite oxides are intriguing nano-materials with a wide range of properties in photocatalysis, electrochemical sensors, and fuel cells. Perovskites synthesized on a nanoscale have already gained a lot of interest for their catalytic properties when utilized as enhancers. The catalytic performance of these oxides is larger than that of other transition metal compositions as well as some noble metal oxides. Electrical conductivity, electroactive structure, mobility of oxide ions across the crystal structure, changes in oxygen concentration, thermal

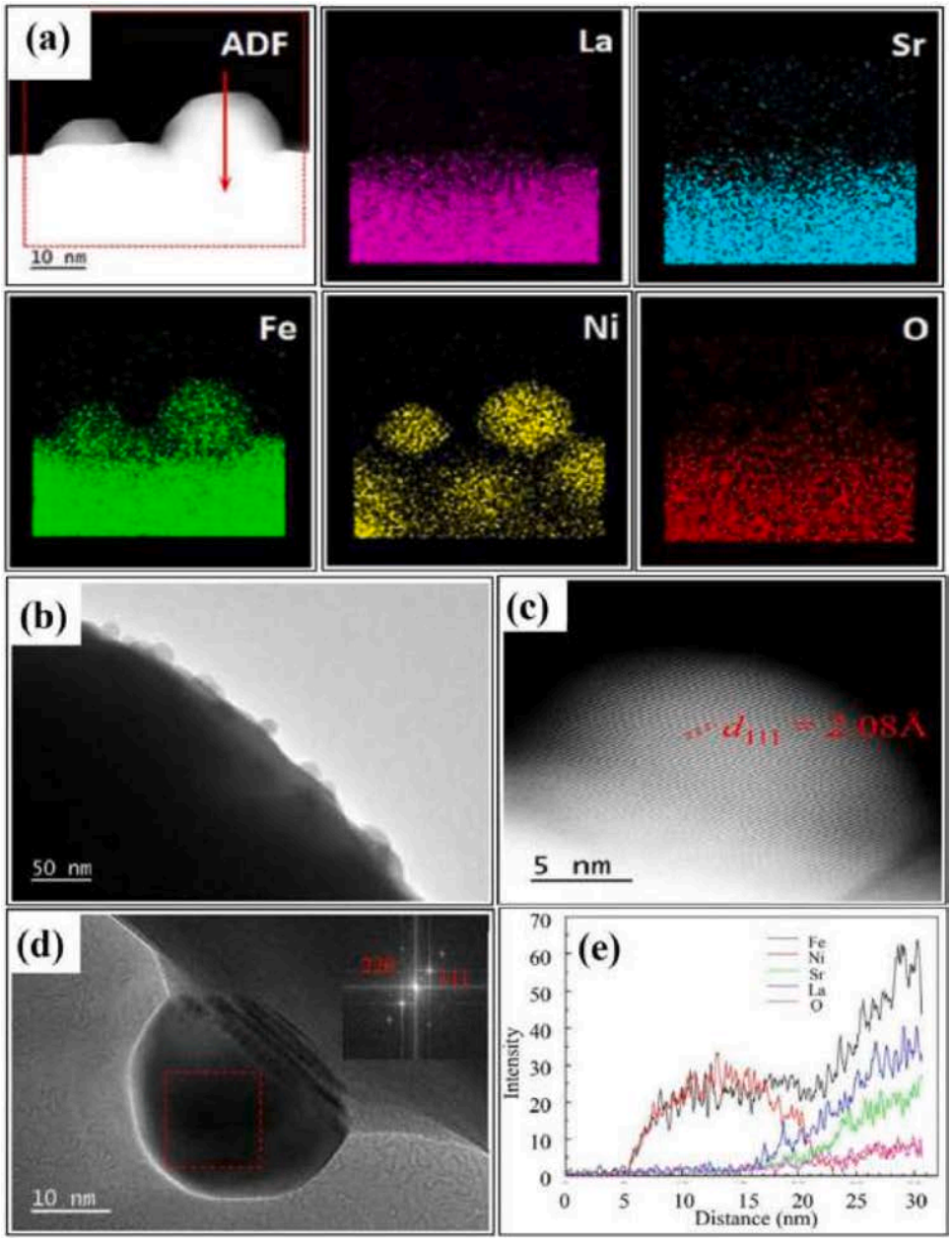

Fig. 5. (a). AFD STEM micrographs and the conforming EDX (b-d). Transition electron micrographs of the $La_{0.6}Sr_{0.4}Fe_{0.9}Ni_{0.1}O_{3-\delta}$ powder (e). the conforming EDS line scanning profiles alongside the arrow categorized in (a) [131].

and chemical stability, and dielectric capabilities are some of the physical and chemical abilities perovskite materials exhibit. We will explore some performance-enhancing strategies for perovskite oxides in this review article, which can improve their characteristics.

4.1. *Interface engineering*

The performance of catalysts can be improved by modifying their surfaces with uniformly dispersed active nanoparticles. Many methods are used to prepare such nanoparticles such as wet-chemistry or PVD. Irvine with his coworkers [126] demonstrated that a rationally controlled composition and non-stoichiometric approach can be used for growing nano-size phases from perovskite oxides. Such non-stoichiometry allows a shift in balance site to create particle exsolution much more active and make the manufacturing of compositionally transformed nano-particles (i.e., metallic, oxides, or mixtures) relatively easy. Also, it tends to offer extraordinary control over particle size distribution and surface modification which has been presented before in the literature [127]. Recently, the same group has demonstrated that lattice strain can be used to attain an abundant amount of exsolution of Ni nano-particles in $La_{0.2}Sr_{0.7}Ni_{0.1}Ti_{0.9}O_{3-\delta}$ perovskite material [128]. Nanoparticles formed on perovskite surfaces are important for many applications such as photocatalysis and recyclable energy. The in-situ nanoparticles produced possess tenability, high electrochemical stability, and coking resistance. The relaxation energy of the misfit strain is attributed to the enhanced lattice strain exsolution process. This research provides a fascinating technique for developing nanostructured materials. Lei Yan et al., in their paper [129] has reported that bilayer electron transfer layer (ETL) SnO_2/ZnO is implemented to achieve less energy loss and wide open-circuit voltage (Voc) for high performing inorganic $CsPbI_2Br$ perovskite solar cells (PVSC). On the SnO_2/ZnO surface, a high-quality $CsPbI_2Br$ film with regular crystal grains and maximal coverage may be produced. The higher-lying conductive band of ZnO stimulates favorable cascade energy level

compatibility between perovskite and SnO_2/ZnO bilayer ETL with enhanced electron extraction capacity thus enhancing perovskite material performance. Through interface engineering of the typical mesoscopic N-I-P configuration, Antonio Agresti and his team have proven the successful implementation of two-dimensional materials such as graphene and functional MoS_2. When compared to normal devices, using 2D materials improves both the stability and overall power conversion efficiency (PCE) of PSCs [130]. Sun and colleagues [131] described a highly active Ni-doped $La_{0.6}Sr_{0.4}FeO_{3-x}$ for LSTFN electrodes fueled by hydrocarbons. Under circumstances identical to those utilized by the cell anode, Ni-Fe nanoparticles with a particle size of about 20 nm were ejected via in situ technique and evenly scattered over the surface of the LSFN particles. Fig. 5 represents the TEM, STEM spitting image, and the conforming EDS of the $La_{0.6}Sr_{0.4}Fe_{0.9}Ni_{0.1}O_{3-\delta}$ powder.

Salim et al., [140] presented an effective and operative interface engineering approach for attaining relatively reliable planar perovskite solar cells (PSCs) engaging SnO_2 electron active films in his publication. A 3-aminopropyltriethoxysilane (APTES) self-assembled monolayer (SAM) was prepared to improve the perovskite/SnO_2-ESL layer contact. Their findings suggest that using an APTES, SAM, and ESL/perovskite interface engineering to make safe, hysteresis-free PSCs is a smart option. The key problem in developing OER catalysts is the stabilization of the active catalytic surface while achieving appropriate high oxygen evolution (OER) performance. Structural instability is frequently associated with the high electrocatalytic activity. $SrRuO_3$ (SRO) perovskite material, is a potential oxygen evolution reaction (OER) catalyst that can dissolve under OER circumstances. Padmanathan et al., [132,133] have described that SRO with a thin film of STO coating functions as a lasting active electrocatalyst. DFT experiments revealed that Ru 4d microelectronic states are created inside the STO bandgap, and the electronic hybridization is modified hence increasing electron transport to the active adsorption species.

There are numerous methods to formulate nano-particles on the perovskite oxide surface. Kim et al., [134] produced Co_3O_4 loaded $Nd_{0.5}Sr_{0.5}CoO_{3-\delta}$ (NSC) catalyst (Opt-NSC@Co_3O_4) with an infiltration method. As a solvent for amalgam Li and Air batteries, this substance has outstanding electrochemical strength and constancy. With the specific microstructure created by the infiltration technique, starting potential, as well as restrictive current density for OER and ORR, are vividly enhanced by systematic study and re-design. Increased electrochemical properties propose that resulting hybrid catalysts produced using the progressive infiltration method could be auspicious materials for organically comprehensive energy-related applications. Yu et al., [135] used diluted HNO_3 to treat the surface of $La_{0.8}Sr_{0.2}MnO_{3-\delta}$ (LSMO). As a result, MnO_x is made on the interface of the LSMO. The ORR performance of MnO_x/LSM heterostructure was therefore increased.

Despite impressive photovoltaic performance with more than 22 percent of energy conversion efficiency, perovskite-based solar cells have very less stability in operation with market requirements far from being met. Various technical techniques for overcoming the problem of instability have been suggested, but while they provide significant incremental gains, they are still far from being a market-proof alternative. Grancini et al., [136] engineered a very firm 2D/3D (HOOC$(CH_2)_4NH_3)_2PbI_4$/$CH_3NH_3PbI_3$ perovskite connection to create stable perovskite products. In carbon-based design, 2D/3D junction generates an outstanding gradual-organized multi-dimensional contact with up to 12.9 percent efficiency.

To improve perovskite solar cell performance, effective interface engineering and device design are intended to improve optoelectronic characteristics and the ions extraction pathway at selected electrodes. To alter the working function (WF) of the perovskite layer and the TiO_2 energy transfer layer (ETL) and create the perovskite / ETL interface, Agresti et al., [137] employed 2D transition metal carbides ($Ti_3C_2T_x$) with variable termination groups (T_x). Incorporating $Ti_3C_2T_x$ to halide perovskite and TiO_2 layers allows the WFs to be tweaked without affecting other electronic characteristics, according to UV light scattering spectroscopy calculations and functional density theory designs. ETL-free perovskite solar cells (PSCs) have developed a lot of concern because of their less cost and easy production technique. However, an additional interface layer has been introduced, resulting in significantly higher efficiency than full-structure PSCs. Li et al., [138] described an in-situ device development methodology for the ionic liquid perovskite precursor methyl ammonium acetate (MAAc) which is considerably distant from the interface engineering procedure in preceding studies.

Performance degradation of perovskite $La_{1-x}Sr_xCoO_{3-\delta}$ (LSC) is produced by changes in the surface arrangement. Feig and colleagues discovered that the $La_{1-x}Sr_xCoO_{3-\delta}$ (LSC) surface's high activity is located only at some scarce active sites. Minute quantities of SrO separated can cause deactivation, while Co, on the other hand, leads to reactivation [139]

Though perovskite light-emitting diodes (P-LEDs) are capable of displays and illumination of the next decade, their performance is still significantly less than that of traditional organic and inorganic equivalents. Noteworthy struggles are needed for achieving high-performance P-LEDs in numerous aspects of the electroluminescence procedure. Salim et al., [140] presented an enhanced modular P-LED framework focused on logical device architecture and interface engineering for energy proficient photon generation and improved light efficiency. The perovskite emitter's interface motivated crystallization and defect passivation is synergistically achieved through altering the underlying interlayer, which results in the dominance of trap-mediated nonradioactive recombination losses.

4.2. Defect engineering

Oxygen Vacancies formed in perovskites allow them to have larger apparent surface-active areas, as shown in spine-structured metal oxides and (oxy) hydroxides. To increase adhesion on the adsorbent surface, O_2 vacancies can alter the electronic configurations of electrocatalysts by increasing the orientation of active metal site members. Furthermore, clustered electrons next to oxygen vacancies are scattered allowing electrons to be transferred from reaction interfaces to electrodes [141]. The presence of oxygen vacancies in perovskite oxides can potentially be employed to adjust OER performance.

The influence of spatial occupancy and oxygen vacancy of B-site cations on the catalytic activity of perovskite $NdNiO_3$ layers were investigated by Wang et al., [142]. Laser beam deposition was used to produce $NdNiO_3$ thin film on a single-crystalline $SrTiO_3$ (STO) (001) surface. The increased ratio of Ni^{3+}/Ni^{2+} is a favorable occupancy for orbital catalytic activity and enough concentration of oxygen vacancies has been reported in this literature.

The creation of elevated OER electrocatalysis is important for many energy-related applications due to the slower reaction kinetics of the oxygen evolution process (OER). Oxygen defect manipulation has been found as a key strategy for controlling the OER behavior of transition metal oxides. However, generating an oxygen defect in a controlled manner remains a tough task, and more study into the influence of oxygen defect on OER dynamics is needed. Using the perovskite thin-film $PrBa_{0.5}Sr_{0.5}Co_{1.5}Fe_{0.5}O_{5+\delta}$ (PBSCF) as a typical substrate, Dutta et al., [143] formed oxygen vacancies of specific quantities in the Ar and H_2 plasma treatment products. Electrochemical studies have shown that the OER production of PBSCF has been considerably enhanced with the introduction of oxygen vacancies.

As related to metal oxides with the vacancies in the anion, cation vacancies are difficult to create. Sn vacancies were also created on the surface of SnCoFe perovskite oxide by Hu and colleagues [144]. As a result of the Sn vacancies, more active Co-Fe sites were revealed, enhancing OER efficiency. Double anion and cation doping are also possibilities. Both the cobalt-free perovskite $SrFeO_{3-\delta}$ (SF) and $SrFe_{0.9}Ti_{0.1}O_{3-\delta}$ (SFT) were doped with fluoride anions [145]. F-doping enhanced bulk diffusion, surface characteristics, and ORR findings in SF.

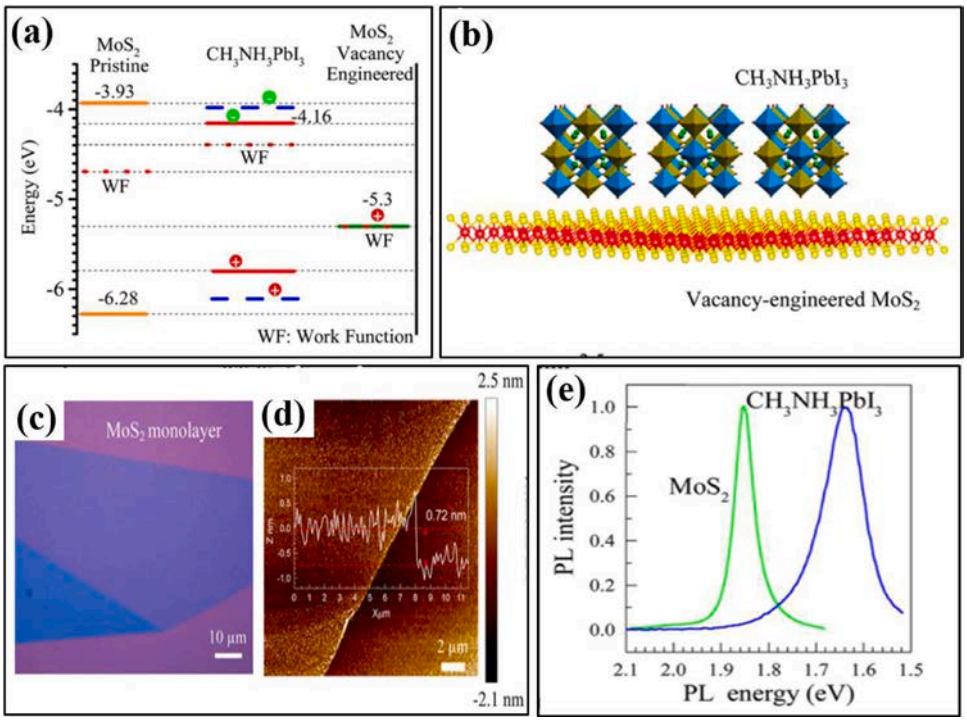

Fig. 6. (a) Band orientation of a pure and vacant position MoS_2 monolayer with $CH_3NH_3PbI_3$ in a diagram. (b) A vacant position $MoS_2/CH_3NH_3PbI_3$ heterostructure is depicted. (c) A 100 m MoS_2 layer on a SiO_2/Si surface as seen under a microscope. (d) Photograph of single-layer MoS_2 on a SiO_2/Si substrate taken with an AFM. The diameter is 0.72 nm, as seen in the inset. Optical properties of mechanically exfoliated MoS_2 monolayer flakes and CH_3NH_3PbI perovskite layers (e) [150].

To comprehend how to govern n-type conductivity, Chen et al., [146] investigated $BaSnO_3$'s defect chemistry using a modular analysis method to hybrid concentration. They demonstrated that in un-doped materials, native defects cannot induce large amounts of n-type conductivity rather adventitious hydrogen existing in materials can act as narrow donors.

The introduction of cesium lead iodide ($CsPbI_3$) perovskite solar cells (PSCs) has attracted the scientific society's interest in photovoltaics. Furthermore, they have low power conversion efficiency due to the existence of impurities. $CsPbI_3$ defect engineering is used to create $CsPbI_3$/Br/InI_3, a novel all-inorganic perovskite material [147]. $CsPbI_3$/Br/InI_3 has remarkable environmental stability in oxygen for more than two months, whereas those focusing on $CsPbI_3$ will only last a few days. The achievement is a significant step forward for all-inorganic PSCs, and it provides the road for additional research to improve efficiency.

The influence of oxygen vacancies on perovskite material performance in the OER was also shown via theoretical experiments. F Tahini et al., used DFT calculations to examine oxygen vacancies in perovskite $SrCoO_3$ for thermal, mechanical, and kinetic problems [148]. They discovered that compressive bending strain can raise surface oxygen vacant energy by up to 25%. The influence of oxygen vacancies on the characteristic of OER on $PrBaCo_2O_6$ double perovskite was investigated by Miao et al., [149]. As the free electrons size increases to $\gamma = 0.5$ the intrinsic OER process is naturally reduced due to the formation of an organized structure in PrO_{1-} layers with an intricate pattern of pyramid $Co^{3+}O^5$ and octahedral $Co^{3+}O^6$, resulting in the electron spin of octahedral Co^{3+}ions changing to LS state from HS state.

The spin-state change causes a large reduction in the eg loading of Co ions, resulting in an increase in electrical resistivity and a drop in the Co-O bond covalence, which has a negative influence on OER kinetics. The efficiency of a photovoltaic system is highly reliant on the absorber layer's light-harvesting performance and the donor/acceptor interface charging separation. Atomically small, two-dimensional transition metal exhibits heavy contact with light and matter, high mobility of electrons, and high optical conductivity therefore, they may be extremely capable materials for optoelectronics and solar cells. Nevertheless, realistic implementations are constrained by the small optical absorption route intrinsic in these atomically thin films. The geometry of the heterostructure consisting of 2-D TMCs (e.g., MoS_2) and a highly absorbent substance with extensive electron-hole dispersion such as methylammonium lead halide perovskite ($CH_3NH_3PbI_3$) can to some degree resolve this restriction. Peng et al., [150] presented the potential to resolve the intrinsic band offset at the $CH_3NH_3PbI_3/MoS_2$ boundary by generating MoS_2 sulfur vacancies utilizing minor plasma treatment. Rapid hole transition from $CH_3NH_3PbI_3$ to MoS_2 occurs within 320 fs with 83 percent photo-excitation performance as illustrated in Fig. 6.

Low-temperature synthesized perovskites have been in the spotlight in recent times due to their unique blend of characteristics such as high absorbance, excellent defect tolerance, long load carrier diffusion lengths, and great potential for usage in semiconductor applications. Low temperature treated perovskite films appear to have a large number of defect disorders, obstructing their device output enhancement. Although different post-treatment approaches have been reported to passivate perovskite surface defects, the serious issue is that defects inside the bulk film cannot be passivized at the same time. Miao et al., [151] established a modern method by concurrently regulating the kinetics of perovskite production and growing the defects (e.g. unsaturated Pb) to produce closely packed perovskite films with small concentrations of defects. The technique is realized by introducing small molecules dependent on cyanine into the precursor to perovskite. This research lays forth a modern approach to further enhance the efficiency of the low-temperature perovskite films produced and the efficiency of the mechanisms involved.

Tahini et al., [152] demonstrated self-passivation of the tin oxide (SnO_x) electron transportation layer (ETL) driven by enforced filling of oxygen vacancies in photovoltaic devices. The oxygen element of SnO_x ETL is tailored by heating in an oxygen environment to manage the intensity of the trap phase for maximum efficiency in electron concentration. The x of SnO_x rises to 1.84 as the oxygen vacancies are gradually

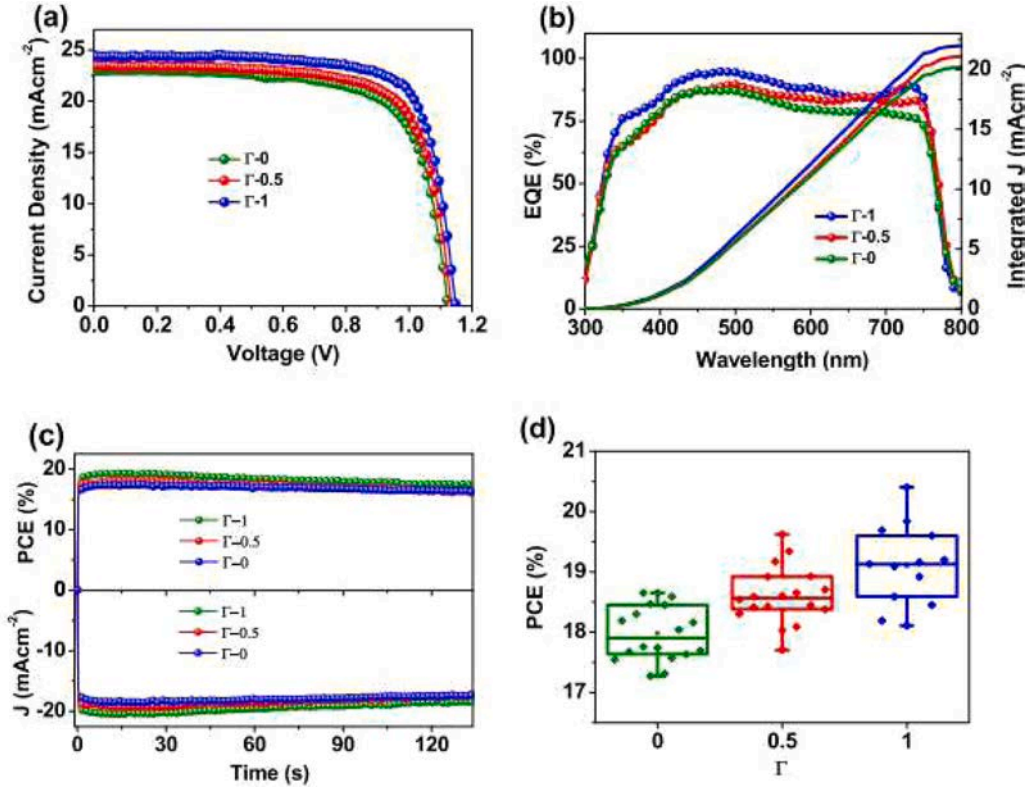

Fig. 7. (a) The JeV (b) EQE curves of the champion devices with different SnOx ETLs, (c) the steady-state output performance of the same set of PSCs, and (d) the box chart of PCEs of the PSCs with different SnOx ETLs [150]. achieving ultrafast.

filled during heating, but the crystalline form develops better to be highly corrosion-resistant. The O_2 treated PSC has a competitive PCE of 21.50 percent, a 1.14 V open-circuit voltage, a short current capability of 24.41 $mAcm^{2,}$ and a fill factor of 73.37 percent. As a result, heating is a rapid and convenient method to determine the efficiency of SnO_x-ETL for high enactment PSCs (Fig. 7).

4.3. Strain modulation

To modulate e_g orbital fracturing and polarity in the octahedral of perovskites and to control oxygen chemical sorption, strain can be used. Cheng et al., [153] observed that the oxygen absorbance of $LaCoO_3$ is prompted by straining. Jiang et al. [154] observed that regulating orbital filling with sufficient plastic strain in the $LaCoO_3$ thin layer improved OER operation significantly. The thin layer was formed with pulsated laser epitaxial (PLE) on (100) oriented $SrTiO_3$ (STO), (LSAT), $(LaAlO_3)_{0.3}(Sr_2AlTaO_6)_{0.7,}$ and $LaAlO_3$ (LAO) perovskites. It is important for the rational design of extremely vigorous perovskite catalysts. Lately, they offer outstanding analysis of the strain-induced nature of oxygen electrocatalysis and ferroelectricity oxides. Strain engineering provides a versatile solution to the design of usable oxides for energy applications [155].

Mixed halide perovskites have proven to be effective light absorbers in photovoltaic panels. Unfortunately, due to the isolation of the framework, these polycrystalline films display inhomogeneity, which leads to lattice distortion or mismatches and eventually in the formation of residual stresses. Through depth-dependent abrasion incidence X-ray scattering abilities, Stoerzinger et al., [156] investigated the evolution of residual strain across the film. The gradient scattering of the perpendicular to the surface in-plane strain part is calculated. In addition, they revealed its influences on carrier subtleties over reliable solar cells, stemming from the strain-induced energy bands twisting the perovskite

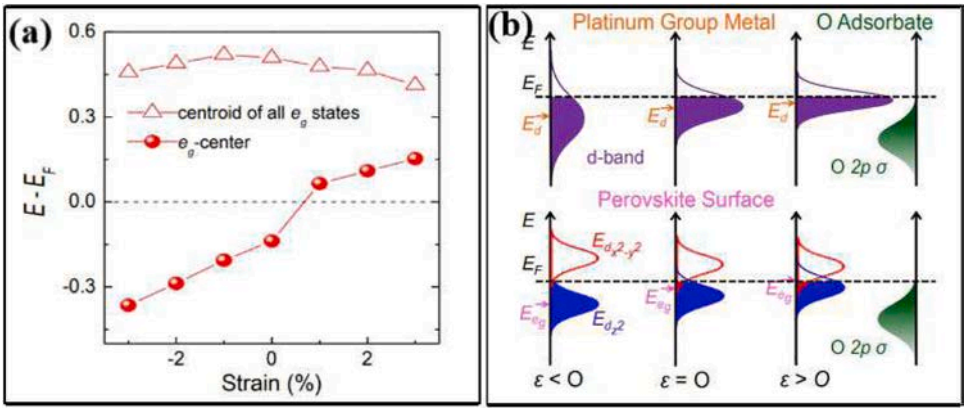

Fig. 8. Strain-induced variations of e_g and D band center (e_d) [157].

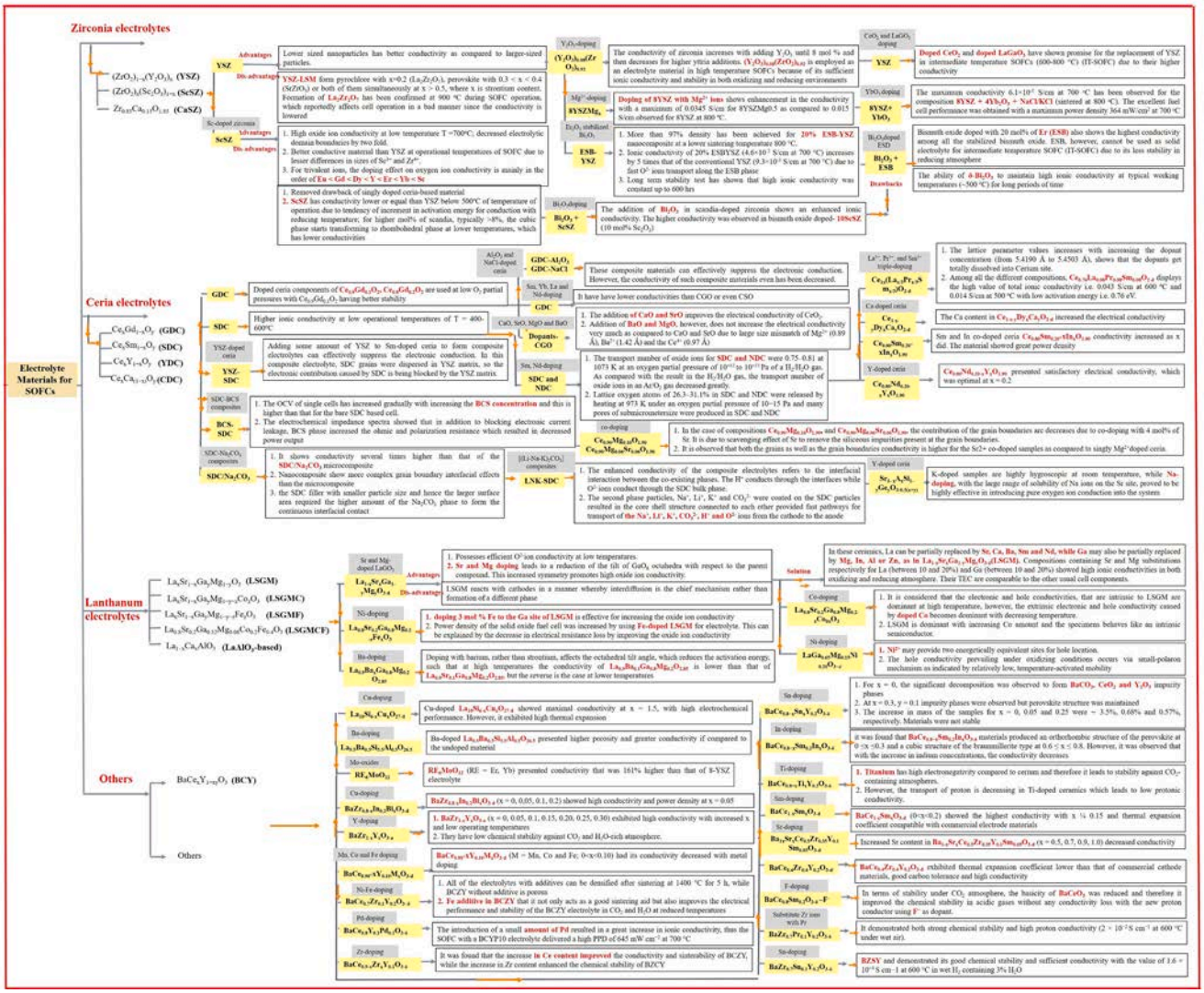

Fig. 9. Summary of Electrolyte materials for solid oxide fuel cells.

absorber.

To assess its effects on both ORR and OER, Petrie et al., [155,157] [155,157] produced the epitaxial strain of $LaNiO_3$ (LNO). The compressive tension has been observed to considerably enhance both processes. The findings have been higher than in noble metals such as platinum since the e_g orbitals were strain-induced to disengage. LNO asymmetries can be significantly affected by orbital separation and polarization (Fig. 8).

Another noteworthy example of strain-induced oxygen deficiency is strontium cobaltite ($SrCoO_x$), which was examined by Petrie et al., [156–158]. They discovered that interfacial tensile strain may be used to adjust the oxygen non-stoichiometry of $SrCoO_x$. The oxygen vacancies formed by tensile strain increase catalytic activity, equivalent to metal oxide IrO_2. By introducing a modest biaxial tensile strain (2%) to cobaltite, the oxygen activation energy barrier is reduced by 30%, resulting in an oxygen-deficient steady state that would not be attained in uncontrolled cobaltite.

5. Future perspective and concluding remarks

Currently, perovskite materials represent the exploited application in the fields of energy storage and conversion devices as these materials are being regarded as key materials in the production of SOFCs. Perovskite-type proton-conducting oxides are considered promising materials for the development SOFCs capable to operate at reduced temperatures owing to higher protonic conductivity than oxygen ions corresponding to smaller ionic sizes. However, according to literature protonic, SOFCs have lower power output values than oxygen-ion-based SOFCs, which could be due to poor sintering of proton-conducting perovskite electrolytes. The lack of a compatible cathode, on the other hand, could be a limiting factor in this dilemma. As the operating temperature drops, the activity of the cathode for ORR falls quickly. Because these cathode materials are composed of perovskite oxides that react easily with similar perovskite-structured based proton conductors, the activity of the cathode for ORR diminishes rapidly as the operational temperature drops.

According to previously reported work in literature, it has been observed that three types of available electrolytes are insufficient and can be obtained by several synthesis methods or from the intrinsic properties of materials. Stabilized ZrO_2 electrolyte characterized by significant physio-chemical stability but poor conductivity at low temperatures which make it insufficient for practical application in IT-SOFCs. Bi_2O_3-based electrolyte materials possess significant conductivity and less stability which limited their use in IT-SOFCs. Doped CeO_2 materials operate sufficiently at a temperature range of 450–600 °C but these materials are associated with internal current issues which limit their applications at higher temperatures The LSGM and other perovskite electrolytes also suffering from stability issues while on the other

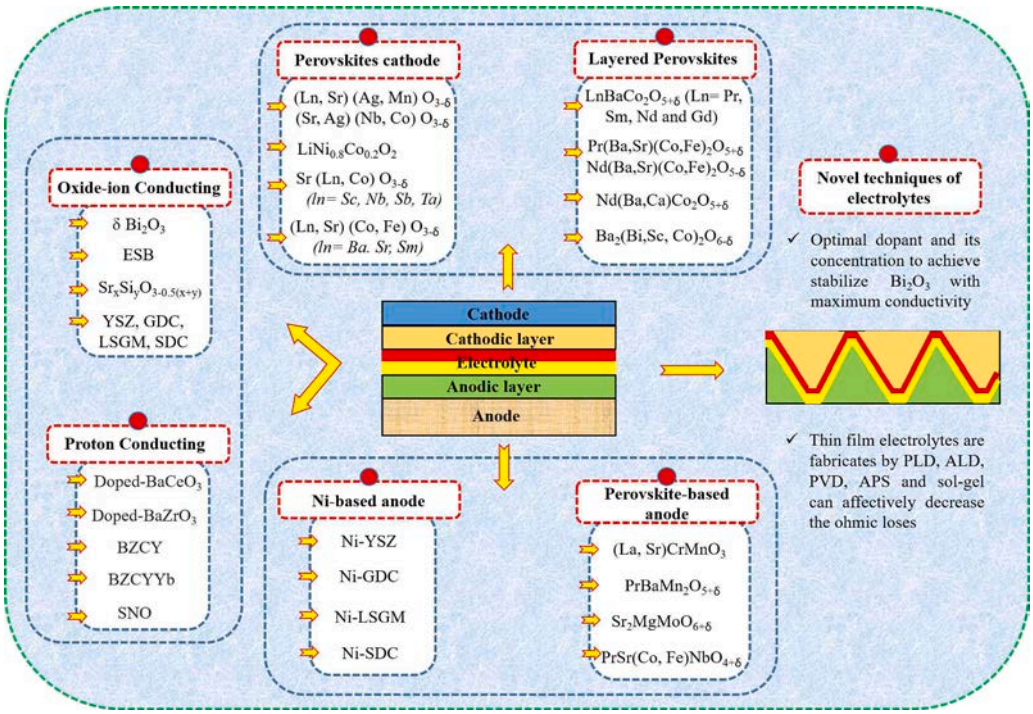

Fig. 10. An optimal setup for perovskite-based materials for LT-SOFCs.

hand electrolyte materials have the potential of proton conduction or dual-conduction can be utilized at a range of low to intermediate temperatures (400–800 °C) owing to less activation energy values. However, these materials can become the first choice for lowest temperature SOFC electrolyte materials by upgrading their physical and chemical stability.

In comparison to oxygen ion conductors, proton conductors facilitate the easiest migration of protons which results in lower activation energy. That's why proton conductors have attracted the attention of researchers as more convenient and suitable electrolytes are being utilized in SOFC at lower temperature ranges. The main network of proton-conducting electrolytes is comprised of perovskite oxides such as $BaZrO_3$ and $BaCeO_3$-based electrolytes. Proton conductors have a downside of lacking stability in an atmosphere comprising of SO_2, CO_2, or H_2O under operating conditions of SOFC. $BaCeO_3$-based electrolyte materials exhibit poor chemical stability but higher proton conductivity however, $BaZrO_3$-based electrolytes show opposite behavior towards $BaCeO_3$-based electrolytes. These materials can be used in combination to develop a new hybrid ($BaCe_xZr_{1-x}O_3$) form for attaining good stability and higher conductivity.

Presently, among various $BaCe_xZr_{1-x}O_3$-based electrolytes, BCZY712 has been studied widely. Several $BaCeO_3$-based electrolytes (such as $BaCe_{0.9}Nd_{0.1}O_{3-\delta}$) materials are regarded as dual ion electrolytes under certain conditions due to the conduction of proton and oxygen ions. Currently, perovskite BZCYYb has been regarded as the best-known dual ion electrolyte among all. CeO_2 and carbonate composites, such as SDC/Na_2CO_3 are well-known examples of dual ion electrolytes. Fuel cells comprising dual ion electrolytes have provided enhanced power output at a lower temperature range. Dual ion electrolytes diminish the use of an external humidification device in the case of D-SOFCs which make the system more reliable and simpler. However, the performance of D-SOFCs at low temperatures can be enhanced by optimizing the electrode materials. Because of differences of these electrolyte materials for oxygen ion conduction, mechanical properties, and chemical stability, it has been concluded that the combined use of these materials can provide enhanced performances such as, by considering the example, doping of thin layer CeO_2 on stabilized ZrO_2 aid to prevent the potential reaction between high-performance cathode materials and stabilized ZrO_2-based electrolyte. Currently, this material is being widely used as the main structure of single cells in various running SOFC stacks. Similarly, the LGSM layer on doped CeO_2 electrolyte prevents the interface reaction between electrode and electrolyte and provides high open-circuit voltage. The combination of both ZrO_2 and δ-Bi_2O_3 ensures the mechanical and chemical properties of electrolyte to prevent the interface reaction, thus play a significant role in promoting the ORR performance at the cathode-electrolyte interface. Electronic conductivity can be blocked by doped CeO_2 layer between anode and δ-Bi_2O_3 to prevent the reduction of δ-Bi_2O_3 at the anode-electrolyte interface

Assembly of triple-layer electrolyte provides complexity in the structure and might be designed for the improvement of ITSOFC performance. Each layer of electrolyte is specific to its function therefore, an approach of utilizing a combination of several electrolyte materials could be a good choice for the development of SOFC. Additionally, the preparation route also plays a significant role in the fabrication of the electrolyte layer. Advanced fabrication techniques such as, pulse laser deposition can minimize the thickness of dense electrolyte layer which in return improve the electrochemical performance of SOFCs. For the time being, the cost of fabrication routes is a major factor for their large-scale applications and quality. However, reduced operating temperatures can cause a major problem by increasing the ASR of the electrode. For commercial applications of IT-SOFCs capable to function at low temperatures, there should be a high-demanding need that cathode materials must be developed synchronously. We have briefly summarized the techniques and dopant strategies to be used in different electrolytes in the Fig. 9 that help us to achieve a maximum power density at low and intermediate temperature SOFCs Fig. 10.

Declaration of Competing Interest

The authors declare that they have no known competing financial interests or personal relationships that could have appeared to influence the work reported in this paper.

Acknowledgement

This work was supported by the National Key Research and Development Program of China (Basic Research Project, Grant No. 2017YFB0306100) and the National Key Research and Development Program of China (China-USA Intergovernmental Cooperation Project, Grant NO. 2017YFE0105900) and Supported by 111 Project 2.0 (BP0618008).

References

[1] Y. Deng, J. Wei, Z. Sun, D. Zhao, Large-pore ordered mesoporous materials templated from non-Pluronic amphiphilic block copolymers, Chem. Soc. Rev. 42 (2013) 4054–4070.
[2] N. Abas, A. Kalair, N. Khan, Review of fossil fuels and future energy technologies, Futures 69 (2015) 31–49.
[3] I. Dincer, C.O. Colpa, Introduction to stationary fuel cells. Solid Oxide Fuel Cells, The Royal Society of Chemistry, 2013, pp. 1–25.
[4] P. Ding, W. Li, H. Zhao, C. Wu, L. Zhao, B. Dong, S. Wang, Review on ruddlesden–popper perovskites as cathode for solid oxide fuel cells, J. Phys. Mater. 4 (2) (2021), 022002.
[5] D.M. Bastidas, S. Tao, J.T. Irvine, A symmetrical solid oxide fuel cell demonstrating redox stable perovskite electrodes, J. Mater. Chem. 16 (2006) 1603–1605.
[6] K.T. Le, C.M. Gore, E.D. Wachsman, Feasibility of low temperature solid oxide fuel cells operating on reformed hydrocarbon fuels, J. Mater. Chem. 22 (2012) 22405–22408.
[7] S.H. Pi, J.W. Lee, S.B. Lee, T.H. Lim, S.J. Park, C.O. Park, R.H. Song, Performance and durability of anode-supported flat-tubular solid oxide fuel cells with Ag-Infiltrated cathodes, J. Nanosci. Nanotechnol. 14 (2014) 7668–7673.
[8] S. Preethi, M. Abhiroop, K.S. Babu, Low temperature densification by lithium co-doping and its effect on ionic conductivity of samarium doped ceria electrolyte, Ceram. Int. 45 (2019) 5819–5828.
[9] J.A. Lane, J.L. Neff, G.M. Christie, Mitigation of the deleterious effect of silicon species on the conductivity of ceria electrolytes, Solid State Ion. 177 (2006) 1911–1915.
[10] H. Shi, C. Su, R. Ran, J. Cao, Z. Shao, Electrolyte materials for intermediate-temperature solid oxide fuel cells, Prog. Nat. Sci. Mater. Int. (2020).
[11] C. Veranitisagul, A. Kaewvilai, W. Wattanathana, N. Koonsaeng, E. Traversa, A. Laobuthee, Electrolyte materials for solid oxide fuel cells derived from metal complexes: gadolinia-doped ceria, Ceram. Int. 38 (3) (2012) 2403–2409.
[12] C. Madhuri, K. Venkataramana, A. Nurhayati, C.V. Reddy, Effect of La^{3+} and Pr^{3+} co-doping on structural, thermal and electrical properties of ceria ceramics as solid electrolytes for IT-SOFC applications, Curr. Appl. Phys. 18 (2018) 1134–1142.
[13] Y.J. Kang, G.M. Choi, The effect of alumina and Cu addition on the electrical properties and the SOFC performance of Gd-doped CeO_2 electrolyte, Solid State Ion. 180 (2009) 886–890.
[14] S.A. Acharya, V.M. Gaikwad, S.W. D'Souza, S.R. Barman, Gd/Sm dopant-modified oxidation state and defect generation in nano-ceria, Solid State Ion. 260 (2014) 21–29.
[15] K. Shan, F.R. Zhai, N. Li, Z.Z. Yi, On the sol-gel synthesis and structure, electronic and ionic conductivities and impedance behavior of Y, Fe Co-Doped $SrTiO_3$ mixed conductor, in: Solid State Phenomena, 281, Trans Tech Publications Ltd, 2018, pp. 774–781.
[16] M. Mogensen, D. Lybye, N. Bonanos, P.V. Hendriksen, F.W. Poulsen, Factors controlling the oxide ion conductivity of fluorite and perovskite structured oxides, Solid State Ion. 174 (2004) 279–286.
[17] Z. Shao, M.O. Tadé, Intermediate-temperature solid oxide fuel cells, Chem. Soc. Rev. 37 (2016) 1568–1578.
[18] B.C. Steele, Appraisal of $Ce_{1-y}Gd_yO_{2-y/2}$ electrolytes for IT-SOFC operation at 500 °C, Solid State Ion. 129 (2000) 95–110.
[19] X. Li, H. Zhao, F. Gao, N. Chen, N. Xu, La and Sc co-doped $SrTiO_3$ as novel anode materials for solid oxide fuel cells, Electrochem. Commun. 10 (2008) 1567–1570.
[20] X. Li, H. Zhao, X. Zhou, N. Xu, Z. Xie, N. Chen, Electrical conductivity and structural stability of La-doped $SrTiO_3$ with a-site deficiency as anode materials for solid oxide fuel cells, Int. J. Hydrog. Energy 35 (2010) 7913–7918.
[21] D.S. Lee, W.S. Kim, S.H. Choi, J. Kim, H.W. Lee, J.H. Lee, Characterization of ZrO_2 co-doped with Sc_2O_3 and CeO_2 electrolyte for the application of intermediate temperature SOFCs, Solid State Ion. 176 (2005) 33–39.
[22] S. Sarat, N. Sammes, A. Smirnova, Bismuth oxide doped scandia-stabilized zirconia electrolyte for the intermediate temperature solid oxide fuel cells, J. Power Sources 160 (2006) 892–896.
[23] C. Xia, Y. Zhang, M. Liu, Composite cathode based on yttria stabilized bismuth oxide for low-temperature solid oxide fuel cells, Appl. Phys. Lett. 82 (2003) 901–903.
[24] E.D. Wachsman, Functionally gradient bilayer oxide membranes and electrolytes, Solid State Ion. 152 (2002) 657–662.
[25] W.H. Kim, H.S. Song, J. Moon, H.W. Lee, Intermediate temperature solid oxide fuel cell using (La, Sr)(Co, Fe) O_3-based cathodes, Solid State Ion. 177 (2006) 3211–3216.
[26] J.A. Kilner, C.D. Waters, The effects of dopant cation-oxygen vacancy complexes on the anion transport properties of non-stoichiometric fluorite oxides, Solid State Ion. 6 (3) (1982) 253–259.
[27] S.P.S. Badwal, F.T. Ciacchi, S. Rajendran, J. Drennan, An investigation of conductivity, microstructure and stability of electrolyte compositions in the system 9 mol%(Sc_2O_3–Y_2O_3)–ZrO_2 (Al_2O_3), Solid State Ion. 109 (3–4) (1998) 167–186.
[28] Y. Chen, N. Orlovskaya, E.A. Payzant, T. Graule, J. Kuebler, A search for temperature induced time-dependent structural transitions in 10 mol% $Sc_2O_{3-\delta}$ mol% CeO_2-ZrO_2 and 8 mol% Y_2O_3-ZrO_2 electrolyte ceramics, J. Eur. Ceram. Soc. 35 (3) (2015) 951–958.
[29] S. Yu, H. Bi, J. Sun, L. Zhu, H. Yu, C. Lu, X. Liu, Effect of grain size on the electrical properties of strontium and magnesium doped lanthanum gallate electrolytes, J. Alloy. Compd. 777 (2019) 244–251.
[30] Y. Ling, F. Wang, L. Zhao, X. Liu, B. Lin, Comparative study of electrochemical properties of different composite cathode materials associated to stable proton conducting $BaZr_{0.7}Pr_{0.1}Y_{0.2}O_{3-\delta}$ electrolyte, Electrochim. Acta 146 (2014) 1–7.
[31] L. Bi, S. Zhang, S. Fang, Z. Tao, R. Peng, W. Liu, A novel anode supported $BaCe_{0.7}Ta_{0.1}Y_{0.2}O_{3-\delta}$ electrolyte membrane for proton-conducting solid oxide fuel cell, Electrochem. Commun. 10 (2008) 1598–1601.
[32] L. Bi, E. Fabbri, Z. Sun, E. Traversa, A novel ionic diffusion strategy to fabricate high-performance anode-supported solid oxide fuel cells (SOFCs) with proton-conducting Y-doped $BaZrO_3$ films, Energy Environ. Sci. 4 (2011) 409–412.
[33] R. Raza, X. Wang, Y. Ma, X. Liu, B. Zhu, Improved ceria-carbonate composite electrolytes, Int. J. Hydrog. Energy 35 (7) (2010) 2684–2688.
[34] R. Singh, S.B. Chavan, Processing and properties of scandia-doped zirconia electrolyte for intermediate temperature SOFC, ECS Trans. 7 (1) (2007) 2207.
[35] M.Y. Shah, S. Rauf, N. Mushtaq, B. Zhu, Z. Tayyab, M. Yousaf, M.B. Hanif, P. D. Lund, L. Lu, M.I. Asghar, Novel perovskite semiconductor based on Co/Fe-codoped LBZY ($La_{0.5}Ba_{0.5}Co_{0.2}Fe_{0.2}Zr_{0.3}Y_{0.3}O_{3-\delta}$) as an electrolyte in ceramic fuel cells, ACS Appl. Energy Mater. (2021).
[36] K. Shaheen, H. Suo, Z. Shah, M.B. Hanif, Z. Hussain, S. Ali, Y. Wang, Electrochemical performance of multifuel based nanocomposite for solid oxide fuel cell, Ceram. Int. 46 (2020) 8832–8838.
[37] K. Shaheen, Z. Shah, H. Gulab, M.B. Hanif, H. Suo, Metal oxide nanocomposites as anode and cathode for low temperature solid oxide fuel cell, Solid State Sci. 102 (2020), 106162.
[38] M.B. Hanif, J.T. Gao, K. Shaheen, Y.P. Wang, M. Yasir, S.L. Zhang, C.X. Li, Performance evaluation of highly active and novel $La_{0.7}Sr_{0.3}Ti_{0.1}Fe_{0.6}Ni_{0.3}O_{3-\delta}$ material both as cathode and anode for intermediate-temperature symmetrical solid oxide fuel cell, J. Power Sources 472 (2020), 228498.
[39] M.B. Hanif, J.T. Gao, K. Shaheen, Y.P. Wang, M. Yasir, C.J. Li, C.X. Li, Highly active and novel Asite deficient symmetric electrode material $(Sr_{0.3}La_{0.7})_{1-x}(Fe_{0.7}Ti_{0.3})_{0.9}Ni_{0.1}O_{3-\delta}$ and its effect on electrochemical performance of SOFCs, Int. J. Hydrog. Energy 46 (2021) 8778–8791.
[40] M.B. Hanif, J.T. Gao, K. Shaheen, Y.P. Wang, M. Yasir, C.J. Li, C.X. Li, Microstructural analysis of highly active cathode material $La_{0.7}Sr_{0.3}Ti_{0.15}Fe_{0.65}Ni_{0.2}O_{3-\delta}$ (LSTFN) by optimizing different processing parameters, Ceram. Int. 47 (2021) 10893–10904.
[41] H. Yang, M.B. Hanif, S.L. Zhang, C.J. Li, C.X. Li, Sintering behavior and electrochemical performance of A-site deficient $Sr_xTi_{0.3}Fe_{0.7}O_{3-\delta}$ oxygen electrodes for solid oxide electrochemical cells, Ceram. Int. 47 (2021) 25051–25058.
[42] M. Hirano, T. Oda, K. Ukai, Y. Mizutani, Effect of Bi_2O_3 additives in *Sc* stabilized zirconia electrolyte on a stability of crystal phase and electrolyte properties, Solid State Ion. 158 (2003) 215–223.
[43] V. Butler, C.R. A.Catlow, B.E.F. Fender, J.H. Harding, Dopant ion radius and ionic conductivity in cerium dioxide, Solid State Ion. 8 (2) (1983) 109–113.
[44] J.A. Kilner, R.J. Brook, A study of oxygen ion conductivity in doped non-stoichiometric oxides, Solid State Ion. 6 (3) (1982) 237–252.
[45] S. Omar, E. D.Wachsman, J.C. Nino, A co-doping approach towards enhanced ionic conductivity in fluorite-based electrolytes, Solid State Ion. 177 (35–36) (2006) 3199–3203.
[46] D.A. Andersson, S.I. Simak, N.V. Skorodumova, I.A. Abrikosov, B. Johansson, Optimization of ionic conductivity in doped ceria, Proc. Natl. Acad. Sci. 103 (10) (2006) 3518–3521.
[47] H. Drings, U. Brossmann, H.D. Carstanjen, Á. Szökefalvi-Nagy, C. Noll, H. E. Schaefer, Enhanced 95Zr diffusion in grain boundaries of nano-crystalline ZrO_2 9.5 mol% Y_2O_3, Phys. Status Solidi (a) 206 (1) (2009) 54–58.
[48] J.T. White, I.E. Reimanis, J. Tong, J.R. O'Brien, A. Morrissey, Internal Reduction of Ni^{2+} in ZrO_2 Stabilized with 10 mol% Y_2O_3 Examined with VSM and SQUID Magnetometry, J. Am. Ceram. Soc. 95 (12) (2012) 4008–4014.
[49] V.V. Milyavskii, A.S. Savinykh, F.A. Akopov, L.B. Borovkova, T.Y.I. Borodina, G. E.E. Val'yano, N.A. Popova, A ceramic based on partially stabilized zirconia: synthesis, structure, and properties under dynamic load, High Temp. 49 (5) (2011) 685–689.
[50] Z. Shao, M.O. Tadé, Intermediate-temperature solid oxide fuel cells, Chem. Soc. Rev. 37 (2016) 1568–1578.
[51] P. Thangadurai, V. Sabarinathan, A. C.Bose, S. Ramasamy, Conductivity behaviour of a cubic/tetragonal phase stabilized nanocrystalline La_2O_3-ZrO_2, J. Phys. Chem. Solids 65 (11) (2004) 1905–1912.
[52] W. Deng, Y. Li, High-temperature electrical properties of polycrystalline MgO-doped ZrO_2, Mater. Res. Bull. 113 (2019) 182–189.
[53] K.P. Padmasree, R.A. Montalvo-Lozano, S.M. Montemayor, A.F. Fuentes, Electrical conduction and dielectric relaxation process in $Ce_{0.8}Y_{0.2}O_{1.9}$ electrolyte system, J. Alloy. Compd. 509 (34) (2011) 8584–8589.

[54] E.D. Wachsman, K.T. Lee, Lowering the temperature of solid oxide fuel cells, Science 334 (2011) 935–939.
[55] Z. Gao, Z. Mao, J. Huang, R. Gao, C. Wang, Z. Liu, Composite cathode $La_{0.15}Bi_{0.85}O_{1.5}$-Ag for intermediate-temperature solid oxide fuel cells, Mater. Chem. Phys. 108 (2008) 290–295.
[56] T. Ishihara, Low temperature solid oxide fuel cells using $LaGaO_3$-based oxide electrolyte on metal support, J. Jpn. Pet. Inst. 58 (2015) 71–78.
[57] R. Pelosato, C. Cristiani, G. Dotelli, S. Latorrata, R. Ruffo, L. Zampori, Co-precipitation in aqueous medium of $La_{0.8}Sr_{0.2}Ga_{0.8}Mg_{0.2}O_{3-\delta}$ via inorganic precursors, J. Power Sources 195 (2010) 8116–8123.
[58] B.A. Khorkounov, H. Näfe, F. Aldinger, Relationship between the ionic and electronic partial conductivities of co-doped LSGM ceramics from oxygen partial pressure dependence of the total conductivity, J. Solid State Electrochem. 10 (2006) 479–487.
[59] Y. Lin, S.A. Barnett, Co-firing of anode-supported SOFCs with thin $La_{0.9}Sr_{0.1}Ga_{0.8}Mg_{0.2}O_{3-\delta}$ electrolytes, Electrochem. Solid State Lett. 9 (2006) A285.
[60] I.N. Sora, R. Pelosato, G. Dotelli, C. Schmid, R. Ruffo, C.M. Mari, The system Al_2O_3 and (Sr, Mg)-doped $LaGaO_3$: phase composition and electrical properties, Solid State Ion. 176 (1–2) (2005) 81–88.
[61] E.K. Shin, E. Anggia, J.S. Park, Effects of Al_2O_3 doping in $BaCeO_3$ on chemical stability and electrical conductivity of proton conducting oxides, Solid State Ion. 339 (2019), 115007.
[62] N.I. Matskevich, T.A. Wolf, The enthalpies of formation of $BaCe_{1-x}RE_xO_{3-\delta}$ (RE= Eu, Tb, Gd), J. Chem. Thermodyn. 42 (2010) 225–228.
[63] H.L. Kim, K.H. Lee, S. Kim, H.L. Lee, Electrical conduction behavior of BaO-doped $LaInO_3$ perovskite oxide, Jpn. J. Appl. Phys. 45 (2R) (2006) 872.
[64] J. Yin, X. Wang, J. Xu, H. Wang, F. Zhang, G. Ma, Ionic conduction in $BaCe_{0.85-x}Zr_xEr_{0.15}O_{3-\alpha}$ and its application to ammonia synthesis at atmospheric pressure, Solid State Ion. 185 (2011) 6–10.
[65] G. Corbel, E. Suard, P. Lacorre, Structural key of the thermal expansion and the oxide ionic conduction in derivatives of La2Mo2O9: a temperature-controlled neutron diffraction study of β-$La_{1.7}Bi_{0.3}Mo_2O_9$, Chem. Mater. 23 (5) (2011) 1288–1298.
[66] J.F. Liu, A.S. Nowick, The incorporation and migration of protons in Nd-doped $BaCeO_3$, Solid State Ion. 50 (1992) 131–138.
[67] A.A. Yaremchenko, V.V. Kharton, E.N. Naumovich, A. A.Tonoyan, V. V. Samokhval, Oxygen ionic transport in Bi_2O_3-based oxides: II. The Bi_2O_3-ZrO_2-Y_2O_3 and Bi_2O_3-Nb_2O_5-Ho_2O= solid solutions, J. Solid State Electrochem. 2 (5) (1998) 308–314.
[68] J. Li, C. Wang, X. Wang, L. Bi, Sintering aids for proton-conducting oxides-a double-edged sword? A mini review, Electrochem. Commun. 112 (2020), 106672.
[69] S. Ćulubrk, V. Lojpur, S. P.Ahrenkiel, J.M. Nedeljković, M.D. Dramićanin, Non-contact thermometry with Dy^{3+} doped $Gd_2Ti_2O_7$ nano-powders, J. Lumin. 170 (2016) 395–400.
[70] S.W. Tao, J.T. Irvine, A stable, easily sintered proton-conducting oxide electrolyte for moderate-temperature fuel cells and electrolyzers, Adv. Mater. 18 (2006) 1581–1584.
[71] J.R. Frade, V.V. Kharton, A. L.Shaula, F.M.B. Marques, Interfacial effects in potentiometric oxygen sensors: the role of transport properties and thickness of solid electrolyte ceramics, Sens. Lett. 6 (3) (2008) 370–380.
[72] Q. Ma, R. Peng, L. Tian, G. Meng, Direct utilization of ammonia in intermediate-temperature solid oxide fuel cells, Electrochem. Commun. 8 (2006) 1791–1795.
[73] Y. Yu, L. Yu, K. Shao, Y. Li, K. Maliutina, W. Yuan, L. Fan, $BaZr_{0.1}Co_{0.4}Fe_{0.4}Y_{0.1}O_3$-SDC composite as quasi-symmetrical electrode for proton conducting solid oxide fuel cells, Ceram. Int. 46 (2020) 11811–11818.
[74] P. Xiaokaiti, T. Yu, A. Yoshida, X. Du, X. Hao, Y. Kasai, G. Guan, Effects of cobalt and iron proportions in $Pr_{0.4}Sr_{0.6}Co_{0.9-x}Fe_xNb_{0.1}O_{3-\delta}$ electrode material for symmetric solid oxide fuel cells, J. Alloy. Compd. (2020), 154738.
[75] C. Zhu, X. Niu, Y. Fu, N. Li, C. Hu, Y. Chen, Y. Ge, Strain engineering in perovskite solar cells and its impacts on carrier dynamics, Nat. Commun. 10 (2019) 1–11.
[76] A. Inoubli, M. Kahlaoui, I. Sobrados, S. Chefi, A. Madani, J. Sanz, A.B.H. Amara, Influence of anionic vacancies on the conductivity of $La_{9.33}Si_{6-x}Al_xO_{26-x/2}$ oxide conductors with an oxyapatite structure, J. Power Sources 271 (2014) 203–212.
[77] Y. Sun, N. Yan, J. Li, H. Wu, J.L. Luo, K.T. Chuang, The effect of calcination temperature on the electrochemical properties of $La_{0.3}Sr_{0.7}Fe_{0.7}Cr_{0.3}O_{3-x}$ (LSFC) perovskite oxide anode of solid oxide fuel cells (SOFCs), Sustain. Energy Technol. Assess. 8 (2014) 92–98.
[78] A. Nakajo, F. Mueller, J. Brouwer, D. Favrat, Mechanical reliability and durability of SOFC stacks. Part II: modelling of mechanical failures during ageing and cycling, Int. J. Hydrog. Energy 3 (2012) 9269–9286.
[79] N. Mahato, A. Banerjee, A. Gupta, S. Omar, K. Balani, Progress in material selection for solid oxide fuel cell technology: a review, Prog. Mater. Sci. 72 (2015) 141–337.
[80] F.S. Da-Silva, T.M. de-Souza, Novel materials for solid oxide fuel cell technologies: a literature review, Int. J. Hydrog. Energy 42 (41) (2017) 26020–26036.
[81] O. Yamamoto, Y. Arachi, H. Sakai, Y. Takeda, N. Imanishi, Y. Mizutani, Y. Nakamura, Zirconia based oxide ion conductors for solid oxide fuel cells, Ionics 4 (1998) 403–408. Kiel.
[82] D. Lee, I. Lee, Y. Jeon, R. Song, Characterization of scandia stabilized zirconia prepared by glycine nitrate process and its performance as the electrolyte for IT-SOFC, Solid State Ion. 176 (2005) 1021–1025.
[83] H. Gu, R. Ran, W. Zhou, Z. Shao, Anode-supported ScSZ-electrolyte SOFC with whole cell materials from combined EDTA–citrate complexing synthesis process, J. Power Sources 172 (2007) 704–712.
[84] G.Y. Cho, Y.H. Lee, S.W. Hong, J. Bae, J. An, Y.B. Kim, S.W. Cha, High-performance thin film solid oxide fuel cells with scandia-stabilized zirconia (ScSZ) thin film electrolyte, Int. J. Hydrog. Energy 40 (2015) 15704–15708.
[85] M. Choi, S. Hwang, S.J. Kim, J. Lee, D. Byun, W. Lee, Rational design of a metallic functional layer for high-performance solid oxide fuel cells, ACS Appl. Energy Mater. 2 (2019) 4059–4068.
[86] Z. Duan, M. Yang, A. Yan, Z. Hou, Y. Dong, Y. Chong, W. Yang, $Ba_{0.5}Sr_{0.5}Co_{0.8}Fe_{0.2}O_{3-\delta}$ as a cathode for IT-SOFCs with a GDC interlayer, J. Power Sources 160 (2006) 57–64.
[87] L.A. Villas-Boas, F.M. Figueiredo, D.P. de-Souza, F.M. Marques, Zn as sintering aid for ceria-based electrolytes, Solid State Ion. 262 (2014) 522–525.
[88] Y. Zheng, M. Zhou, L. Ge, S. Li, H. Chen, L. Guo, Effect of Fe_2O_3 on Sm-doped ceria system solid electrolyte for IT-SOFCs, J. Alloy. Compd. 509 (2011) 546–550.
[89] K. Tanwar, N. Jaiswal, D. Kumar, O. Parkash, Synthesis & characterization of Dy and Ca Co-doped ceria based solid electrolytes for IT-SOFCs, J. Alloy. Compd. 684 (2016) 683–690.
[90] L. Fan, Y. Wang, Z. Jia, Y. Xiong, M.E. Brito, Nanofiber-structured SSC-GDC composite cathodes for a LSGM electrolyte-based IT-SOFCs, Ceram. Int. 41 (2015) 6583–6588.
[91] Z. Zhu, W. Sun, Z. Shi, W. Liu, Proton-conducting solid oxide fuel cells with yttrium-doped barium zirconate electrolyte films sintered at reduced temperatures, J. Alloy. Compd. 658 (2016) 716–720.
[92] H. Matsumoto, Y. Kawasaki, N. Ito, M. Enoki, T. Ishihara, Relation between electrical conductivity and chemical stability of $BaCeO_3$-based proton conductors with different trivalent dopants, Electrochem. Solid State Lett. 10 (2007) B77.
[93] Y. Liu, R. Ran, S. Li, Y. Jiao, M.O. Tade, Z. Shao, Significant performance enhancement of yttrium-doped barium cerate proton conductor as electrolyte for solid oxide fuel cells through a Pd ingressegress approach, J. Power Sources 257 (2014) 308–318.
[94] L. Bi, S. Fang, Z. Tao, S. Zhang, R. Peng, W. Liu, Influence of anode pore forming additives on the densification of supported $BaCe_{0.7}Ta_{0.1}Y_{0.2}O_{3-\delta}$ electrolyte membranes based on a solid-state reaction, J. Eur. Ceram. Soc. 29 (2009) 2567–2573.
[95] H. Iwahara, T. Esaka, H. Uchida, N. Maeda, Proton conduction in sintered oxides and its application to steam electrolysis for hydrogen production, Solid State Ion. 3 (1981) 359–363.
[96] D.A. Medvedev, J.G. Lyagaeva, E.V. Gorbova, A.K. Demin, P. Tsiakaras, Advanced materials for SOFC application: strategies for the development of highly conductive and stable solid oxide proton electrolytes, Prog. Mater. Sci. 75 (2016) 38–79.
[97] F. Gonell, C.M. Sanchez-Sanchez, V. Vivier, C. Laberty-Robert, D. Portehault, Experimental descriptors for the synthesis of multicationic nickel perovskite nanoparticles for oxygen reduction, ACS Appl. Nano Mater. 3 (8) (2020) 7482–7489.
[98] P. Pasierb, M. Osiadły, S. Komornicki, M. Rekas, Structural and electrical properties of BaCe (Ti, Y) O_3 protonic conductors, J. Power Sources 196 (2011) 6205–6209.
[99] F. Su, C. Xia, R. Peng, Novel fluoride-doped barium cerate applied as stable electrolyte in proton conducting solid oxide fuel cells, J. Eur. Ceram. Soc. 35 (2015) 3553–3558.
[100] C. Peng, J. Melnik, J.L. Luo, A.R. Sanger, K.T. Chuang, $BaZr_{0.8}Y_{0.2}O_{3-\delta}$ electrolyte with and without ZnO sintering aid: preparation and characterization, Solid State Ion. 181 (2010) 1372–1377.
[101] D. Gao, R. Guo, Structural and electrochemical properties of yttrium-doped barium zirconate by addition of CuO, J. Alloy. Compd. 493 (2010) 288–293.
[102] Y. Guo, Y. Lin, R. Ran, Z. Shao, Zirconium doping effect on the performance of proton-conducting $BaZryCe_{0.8-y}Y_{0.2}O_{3-\delta}$ ($0.0 \leq y \leq 0.8$) for fuel cell applications, J. Power Sources 193 (2009) 400–407.
[103] E. Fabbri, L. Bi, H. Tanaka, D. Pergolesi, E. Traversa, Chemically stable Pr and Y co-doped barium zirconate electrolytes with high proton conductivity for intermediate-temperature solid oxide fuel cells, Adv. Funct. Mater. 21 (2011) 158–166.
[104] Y. Liu, Y. Guo, R. Ran, Z. Shao, A new neodymium-doped $BaZr_{0.8}Y_{0.2}O_{3-\delta}$ as potential electrolyte for proton-conducting solid oxide fuel cells, J. Memb. Sci. 415 (2012) 391–398.
[105] Y. Guo, R. Ran, Z. Shao, Optimizing the modification method of zinc-enhanced sintering of $BaZr_{0.4}Ce_{0.4}Y_{0.2}O_{3-\delta}$-based electrolytes for application in an anode-supported protonic solid oxide fuel cell, Int. J. Hydrog. Energy 35 (2010) 5611–5620.
[106] L. Yang, S. Wang, K. Blinn, M. Liu, Z. Liu, Z. Cheng, M. Liu, Enhanced sulfur and coking tolerance of a mixed ion conductor for SOFCs: $baZr_{0.1}Ce_{0.7}Y_{0.2-x}Yb_xO_{3-\delta}$, Science 326 (2009) 126–129.
[107] C. Zhou, J. Sunarso, Y. Song, J. Dai, J. Zhang, B. Gu, Z. Shao, New reduced-temperature ceramic fuel cells with dual-ion conducting electrolyte and triple-conducting double perovskite cathode, J. Mater. Chem. A 7 (2019) 13265–13274.
[108] J.R. Petrie, V.R. Cooper, J.W. Freeland, T.L. Meyer, Z. Zhang, D.A. Lutterman, H. N. Lee, Enhanced bifunctional oxygen catalysis in strained $LaNiO_3$ perovskites, J. Am. Chem. Soc. 138 (2016) 2488–2491.
[109] A. Inoubli, M. Kahlaoui, I. Sobrados, S. Chefi, A. Madani, J. Sanz, A.B. Amara, Influence of anionic vacancies on the conductivity of $La_{9.33}Si_{6-x}Al_xO_{26-x/2}$ oxide conductors with an oxyapatite structure, J. Power Sources 271 (2014) 203–212.
[110] H. Mieda, A. Mineshige, A. Saito, T. Yazawa, H. Yoshioka, R. Mori, Influence of nano-sized LSCF cathode and its firing temperature on electrochemical

performance in oxygen-excess-type solid electrolyte (OESE)-based fuel cells, J. Power Sources 272 (2014) 422–426.
[111] C.V. Ramana, M. Bandi, A.N. Nair, F.S. Manciu, S. Sreenivasan, V. Shutthanandan, Electronic Structure, Chemical Bonding, and Electrocatalytic Activity of $Ba(Fe_{0.7}Ta_{0.3})O_{3-\delta}$ Compounds, ACS Appl. Energy Mater. 4 (2) (2021) 1313–1322.
[112] A. Magrasó, M.L. Fontaine, Y. Larring, R. Bredesen, G.E. Syvertsen, H.L. Lein, T. Norby, Development of proton conducting SOFCs based on $LaNbO_4$ electrolyte-status in Norway, Fuel Cells 11 (2011) 17–25.
[113] B. Lin, S. Wang, X. Liu, G. Meng, Stable proton-conducting Ca-doped $LaNbO_4$ thin electrolyte-based protonic ceramic membrane fuel cells by in situ screen printing, J. Alloy. Compd. 478 (2009) 355–357.
[114] S. Baskaran, C.A. Lewinsohn, Y.S. Chou, M. Qian, J.W. Stevenson, T.R. Armstrong, Mechanical properties of alkaline earth-doped lanthanum gallate, J. Mater. Sci. 34 (1999) 3913–3922.
[115] F. Zhang, Q. Yang, B. Pan, R. Xu, H. Wang, G. Ma, Proton conduction in $La_{0.9}Sr_{0.1}Ga_{0.8}Mg_{0.2}O_{3-\alpha}$ ceramic prepared via microemulsion method and its application in ammonia synthesis at atmospheric pressure, Mater. Lett. 61 (2007) 4144–4148.
[116] I.A. Amar, R. Lan, C.T. Petit, S. Tao, Solid-state electrochemical synthesis of ammonia: a review, J. Solid State Electrochem. 15 (2011) 1845.
[117] C. Chen, G. Ma, Preparation, proton conduction, and application in ammonia synthesis at atmospheric pressure of $La_{0.9}Ba_{0.1}Ga_{1-x}Mg_xO_{3-\alpha}$, J. Mater. Sci. 43 (2008) 5109–5114.
[118] Z. Li, R. Liu, J. Wang, Z. Xu, Y. Xie, B. Wang, Preparation of double-doped $BaCeO_3$ and its application in the synthesis of ammonia at atmospheric pressure, Sci. Technol. Adv. Mater. 8 (2007) 566.
[119] P. Ranran, W. Yan, Y. Lizhai, M. Zongqiang, Electrochemical properties of intermediate-temperature SOFCs based on proton conducting Sm-doped $BaCeO_3$ electrolyte thin film, Solid State Ion. 177 (2006) 389–393.
[120] D. Pergolesi, E. Fabbri, E. Traversa, Chemically stable anode-supported solid oxide fuel cells based on Y-doped barium zirconate thin films having improved performance, Electrochem. Commun. 12 (2010) 977–980.
[121] Z. Sun, E. Fabbri, L. Bi, E. Traversa, Lowering grain boundary resistance of $BaZr_{0.8}Y_{0.2}O_{3-\delta}$ with $LiNO_3$ sintering-aid improves proton conductivity for fuel cell operation, Phys. Chem. Chem. Phys. 13 (2011) 7692–7700.
[122] K. Xie, R. Yan, X. Chen, D. Dong, S. Wang, X. Liu, G. Meng, A new stable $BaCeO_3$-based proton conductor for intermediate-temperature solid oxide fuel cells, J. Alloy. Compd. 47 (2009) 551–555.
[123] Z. Li, R. Liu, Y. Xie, S. Feng, J. Wang, A novel method for preparation of doped $Ba_3(Ca_{1.18}Nb_{1.82})O_{9-\delta}$: application to ammonia synthesis at atmospheric pressure, Solid State Ion. 176 (2005) 1063–1066.
[124] Y. Lin, R. Ran, Y. Guo, W. Zhou, R. Cai, J. Wang, Z. Shao, Proton-conducting fuel cells operating on hydrogen, ammonia and hydrazine at intermediate temperatures, Int. J. Hydrog. Energy 35 (2010) 2637–2642.
[125] J. Liu, Y. Li, W. Wang, H. Wang, F. Zhang, G. Ma, Proton conduction at intermediate temperature and its application in ammonia synthesis at atmospheric pressure of $BaCe_{1-x}Ca_xO_{3-\alpha}$, J. Mater. Sci. 45 (2010) 5860–5864.
[126] E.A.R. Assirey, Perovskite synthesis, properties and their related biochemical and industrial application, Saudi Pharm. J. 27 (6) (2019) 817–829.
[127] S.M. Imran, G.N. Shao, M.S. Haider, H.J. Hwang, Y.H. Choa, M. Hussain, H. T. Kim, Carbon nanotube-based thermoplastic polyurethane-poly (methyl methacrylate) nanocomposites for pressure sensing applications, Polym. Eng. Sci. 56 (2016) 1031–1036.
[128] I.A. Kovács, K. Luck, K. Spirohn, Y. Wang, C. Pollis, S. Schlabach, A.L. Barabási, Network-based prediction of protein interactions, Nat. Commun. 10 (2019) 1–8.
[129] X. Zhang, Y. Zhou, Y. Li, J. Sun, X. Lu, X. Gao, J.M. Liu, Efficient and carbon-based hole transport layer-free $CsPbI_2Br$ planar perovskite solar cells using PMMA modification, J. Mater. Chem. C 7 (2019) 3852–3861.
[130] A. Agresti, S. Pescetelli, A.L. Palma, B. Martín-García, L. Najafi, S. Bellani, A. Di-Carlo, Two-dimensional material interface engineering for efficient perovskite large-area modules, ACS Energy Lett. 4 (2019) 1862–1871.
[131] C. Sun, J.A. Alonso, J. Bian, Recent advances in perovskite-type oxides for energy conversion and storage applications, Adv. Energy Mater. 11 (2021), 2000459.
[132] N. Padmanathan, H. Shao, D. McNulty, C. O'Dwyer, K.M. Razeeb, Hierarchical $NiO\text{-}In_2O_3$ microflower (3D)/nanorod (1D) hetero-architecture as a supercapattery electrode with excellent cyclic stability, J. Mater. Chem. A 4 (2016) 4820–4830.
[133] A.R. Akbashev, L. Zhang, J.T. Mefford, J. Park, B. Butz, H. Luftman, A. Vojvodic, Activation of ultrathin $SrTiO_3$ with subsurface $SrRuO_3$ for the oxygen evolution reaction, Energy Environ. Sci. 11 (2018) 1762–1769.
[134] J. Kim, O. Gwon, O. Kwon, J. Mahmood, C. Kim, Y. Yang, G. Kim, Synergistic coupling derived cobalt oxide with nitrogenated holey two-dimensional matrix as an efficient bifunctional catalyst for metal-air batteries, ACS Nano 13 (2019) 5502–5512.
[135] J. Yu, D. Chen, M. Saccoccio, K. Lam, F. Ciucci, Promotion of oxygen reduction with both amorphous and crystalline MnO_x through the surface engineering of $La_{0.8}Sr_{0.2}MnO_{3-\delta}$ Perovskite, ChemElectroChem 5 (2018) 1105–1112.
[136] G. Grancini, C. Roldán-Carmona, I. Zimmermann, E. Mosconi, X. Lee, D. Martineau, M.K. Nazeeruddin, One-Year stable perovskite solar cells by 2D/3D interface engineering, Nat. Commun. 8 (2017) 1–8.
[137] A. Agresti, A. Pazniak, S. Pescetelli, A. Di-Vito, D. Rossi, A. Pecchia, D. Saranin, Titanium-carbide MXenes for work function and interface engineering in perovskite solar cells, Nat. Mater. 18 (2019) 1228–1234.
[138] D. Li, L. Chao, C. Chen, X. Ran, Y. Wang, T. Niu, L. Song, In situ interface engineering for highly efficient electron-transport-layer-free perovskite solar cells, Nano Lett. 20 (2020) 5799–5806.
[139] G.M. Rupp, A.K. Opitz, A. Nenning, A. Limbeck, J. Fleig, Real-time impedance monitoring of oxygen reduction during surface modification of thin film cathodes, Nat. Mater. 16 (2017) 640–645.
[140] K.M. Salim, E. Hassanabadi, S. Masi, A.F. Gualdron-Reyes, M. Franckevicius, A. Devizis, I. Mora-Sero, Optimizing performance and operational stability of $CsPbI_3$ quantum-dot-based light-emitting diodes by interface engineering, ACS Appl. Electron. Mater. 2 (8) (2020) 2525–2534.
[141] J. Bao, X. Zhang, B. Fan, J. Zhang, M. Zhou, W. Yang, Y. Xie, Ultrathin spinel-structured nanosheets rich in oxygen deficiencies for enhanced electrocatalytic water oxidation, Angew. Chem. 127 (2015) 7507–7512.
[142] Y. Wang, Y. Zhang, Z. Liu, C. Xie, S. Feng, D. Liu, S. Wang, Layered double hydroxide nanosheets with multiple vacancies obtained by dry exfoliation as highly efficient oxygen evolution electrocatalysts, Angew. Chem. Int. Ed. 56 (2017) 5867–5871.
[143] A. Dutta, S. Mutyala, A.K. Samantara, S. Bera, B.K. Jena, N. Pradhan, Synergistic effect of inactive iron oxide core on active nickel phosphide shell for significant enhancement in oxygen evolution reaction activity, ACS Energy Lett. 3 (2017) 141–148.
[144] C. Hu, X. Wang, T. Yao, T. Gao, J. Han, X. Zhang, B. Song, Enhanced electrocatalytic oxygen evolution activity by tuning both the oxygen vacancy and orbital occupancy of B-Site metal cation in $NdNiO_3$, Adv. Funct. Mater. 29 (2019), 1902449.
[145] Y. Zhu, X. Zhong, S. Jin, H. Chen, Z. He, Q. Liu, Y. Chen, Oxygen defect engineering in double perovskite oxides for effective water oxidation, J. Mater. Chem. A 8 (2020) 10957–10965.
[146] D. Chen, M. Qiao, Y.R. Lu, L. Hao, D. Liu, C.L. Dong, S. Wang, Preferential cation vacancies in perovskite hydroxide for the oxygen evolution reaction, Angew. Chem. Int. Ed. 57 (2018) 8691–8696.
[147] Z. Zhang, Y. Zhu, Y. Zhong, W. Zhou, Z. Shao, Anion doping: a new strategy for developing high-performance perovskite-type cathode materials of solid oxide fuel cells, Adv. Energy Mater. 7 (2017), 1700242.
[148] D.O. Scanlon, Defect engineering of $BaSnO_3$ for high-performance transparent conducting oxide applications, Phys. Rev. B 87 (2013), 161201.
[149] J. Liang, X. Han, J.H. Yang, B. Zhang, Q. Fang, J. Zhang, J. Lou, Defect-engineering-enabled high-efficiency all-inorganic perovskite solar cells, Adv. Mater. 31 (2019), 1903448.
[150] B. Peng, G. Yu, Y. Zhao, Q. Xu, G. Xing, X. Liu, K.P. Loh, Achieving ultrafast hole transfer at the monolayer MoS_2 and $CH_3NH_3PbI_3$ perovskite interface by defect engineering, ACS Nano 10 (2016) 6383–6391.
[151] X. Miao, L. Wu, Y. Lin, X. Yuan, J. Zhao, W. Yan, L. Shi, The role of oxygen vacancies in water oxidation for perovskite cobalt oxide electrocatalysts: are more better, Chem. Commun. 55 (2019) 1442–1445.
[152] H.A. Tahini, X. Tan, U. Schwingenschlögl, S.C. Smith, Formation and migration of oxygen vacancies in $SrCoO_3$ and their effect on oxygen evolution reactions, ACS Catal. 6 (2016) 5565–5570.
[153] J. Cheng, H. Zhang, S. Zhang, D. Ouyang, Z. Huang, M.K. Nazeeruddin, W. C. Choy, Highly efficient planar perovskite solar cells achieved by simultaneous defect engineering and formation kinetic control, J. Mater. Chem. A 6 (2018) 23865–23874.
[154] E. Jiang, J. Yan, Y. Ai, N. Li, B. Yan, Y. Zeng, J. Ye, Defect engineering of oxygen vacancies in SnO_x electron transporting layer for perovskite solar cells, Mater. Today Energy 12 (2019) 389–397.
[155] A. Kushima, S. Yip, B. Yildiz, Competing strain effects in reactivity of $LaCoO_3$ with oxygen, Phys. Rev. B 82 (2010), 115435.
[156] K.A. Stoerzinger, W.S. Choi, H. Jeen, H.N. Lee, Y. Shao-Horn, Role of strain and conductivity in oxygen electrocatalysis on $LaCoO_3$ thin films, J. Phys. Chem. Lett. 6 (2015) 487–492.
[157] J.R. Petrie, V.R. Cooper, J.W. Freeland, T.L. Meyer, Z. Zhang, D.A. Lutterman, H. N. Lee, Enhanced bifunctional oxygen catalysis in strained $LaNiO_3$ perovskites, J. Am. Chem. Soc. 138 (2016) 2488–2491.
[158] M.B. Hanif, M. Motola, S. Rauf, C.J. Li, C.X. Li, Recent advancements, doping strategies and the future perspective of perovskite-based Solid oxide fuel cells for energy conversion, Chem. Eng. J. 428 (2021), 132603.